

# Development of Discontinuous Galerkin Method for Nonlocal Linear Elasticity

by

Ram Bala Chandran


B.Tech., Mechanical Engineering  
Indian Institute of Technology, Madras (2005)

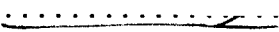
Submitted to the The School of Engineering  
in partial fulfillment of the requirements for the degree of  
Master of Science in Computation for Design and Optimization  
at the

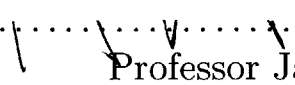
MASSACHUSETTS INSTITUTE OF TECHNOLOGY

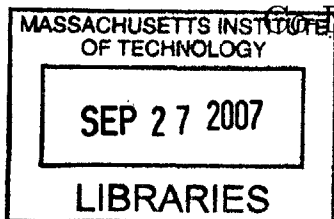
September 2007

© Massachusetts Institute of Technology 2007. All rights reserved.

Author .....  .....  
The School of Engineering  
July 6, 2007

Thesis Supervisor .....  .....  
Professor Raúl Radovitzky  
Department of Aeronautics and Astronautics

Accepted by .....  .....  
Professor Jaime Peraire  
Department of Aeronautics and Astronautics  
Director, Computation for Design and Optimization Program



BARKER



# Development of Discontinuous Galerkin Method for Nonlocal Linear Elasticity

by

Ram Bala Chandran

Submitted to the The School of Engineering  
on July 6, 2007, in partial fulfillment of the  
requirements for the degree of  
Master of Science in Computation for Design and Optimization

## Abstract

A number of constitutive theories have arisen describing materials which, by nature, exhibit a non-local response. The formulation of boundary value problems, in this case, leads to a system of equations involving higher-order derivatives which, in turn, results in requirements of continuity of the solution of higher order. Discontinuous Galerkin methods are particularly attractive toward this end, as they provide a means to naturally enforce higher interelement continuity in a weak manner without the need of modifying the finite element interpolation.

In this work, a discontinuous Galerkin formulation for boundary value problems in small strain, non-local linear elasticity is proposed. The underlying theory corresponds to the phenomenological strain-gradient theory developed by Fleck and Hutchinson within the Toupin-Mindlin framework. The single-field displacement method obtained enables the discretization of the boundary value problem with a conventional continuous interpolation inside each finite element, whereas the higher-order interelement continuity is enforced in a weak manner. The proposed method is shown to be consistent and stable both theoretically and with suitable numerical examples.

Thesis Supervisor: Professor Raúl Radovitzky  
Department of Aeronautics and Astronautics



## Acknowledgments

I would like to thank my advisor, Prof. Raul Radovitzky, for his guidance, patience, and support. I am also greatly thankful to my advisor for making my stay at MIT fun, challenging and for getting me into using and appreciating open-source software.

I am thankful for the support of the DoE through the CalTech ASC Center for Simulation of Dynamic Response of Materials under contract 82-1052904.

I would always be grateful to my undergraduate advisors Prof. M.S Sivakumar and Dr. C.V.Krishnamurthy at IIT Madras for inspiring and making me believe that i am capable of doing research.

I am grateful to my program co-directors, Prof. Jaime Peraire and Prof. Robert Freund for starting and running the most amazing program at MIT.

I would like to thank my graduate administrators, Laura Rose and Laura Koller for essentially making me not worry about any paper work at MIT. My great appreciation to Brian, our lab administrative assistant for feeding me with Indian food during our group meetings.

I shall always be grateful to Dr. Ludovic Noels, University of Liège-Belgium, for 'baby-sitting' me from time to time, for always being there on Yahoo messenger to help me out, and for being one of the most important source of motivation and inspiration at MIT.

Words would do no justice-to the help, motivation and of-course all the football videos ,espresso shots and loads of debugging help from my labmates, Dr. Antoine Jerusalem and Dr. Nayden Kambuchev. I am grateful to my labmates Sudhir and Ganesh for not eating my "Mexican-beauty" pizzas in the group meetings. I am thankful to all my office mates at building 41 for putting up with me for two years.

All this would not have been possible but for the sacrifices, encouragement and motivation from my parents, my sister Rohini and my family back in India and in the US.

I would like to thank my friends at MIT - Ashish, Anshuman, Chetan, Deep, Dipanjan, Harish, Pranava, Sangeeth, Sandeep, Vikas and the entire sangam-brothers gang for making my stay at MIT fun and memorable.

Finally, I would like to thank my friends Adarsh, Krishna, Shankar, Srevatsan and Satyashree for suggesting to me that I cite their respective publications in atleast my acknowledgments and for being there when I needed you guys the most.



# Contents

<b>1</b>	<b>Introduction</b>	<b>13</b>
<b>2</b>	<b>A low order discontinuous Galerkin method for finite hyperelasticity</b>	<b>17</b>
2.1	Motivation . . . . .	17
2.2	Discontinuous Galerkin formulation . . . . .	18
2.3	Finite Element Implementation . . . . .	24
2.4	Numerical Results . . . . .	26
<b>3</b>	<b>A discontinuous Galerkin formulation for linear nonlocal elasticity</b>	<b>31</b>
3.1	Toupin-Mindlin strain-gradient theory of linear elasticity . . . . .	31
3.2	Discontinuous Galerkin formulation . . . . .	36
3.3	Theoretical stability and convergence . . . . .	44
3.3.1	Consistency . . . . .	44
3.3.2	Stability . . . . .	46
3.3.3	Convergence Rate . . . . .	49
3.4	Finite Element Implementation . . . . .	50
<b>4</b>	<b>Numerical tests and examples</b>	<b>59</b>

4.1	Tension Test . . . . .	60
4.2	Bi-material tensile test . . . . .	61
4.3	Clamped Beam under bending loading . . . . .	65
4.4	Size effects under torsion . . . . .	68
<b>5</b>	<b>Conclusions</b>	<b>73</b>
<b>A</b>	<b>Strain Gradient Constitutive Relations</b>	<b>83</b>
<b>B</b>	<b>Derivation of the upper bound of the bilinear form</b>	<b>85</b>
<b>C</b>	<b>Convergence Analysis- discontinuous Galerkin method</b>	<b>91</b>
<b>D</b>	<b>Implementation of second order derivatives of the element shape functions</b>	<b>95</b>
<b>E</b>	<b>Analytical solutions for 1-D strain gradient problems</b>	<b>99</b>
E.1	Uni-axial tensile load . . . . .	99
E.2	Bi-material subjected to uni-axial tensile load . . . . .	100



# List of Figures

2.1	Convergence Analysis of the discontinuous Galerkin method applied to the cantilever beam problem in small deformation. The plot shows the error $v/s$ mesh size $h$ for $\beta = 1.5, 3, 15$ . . . . .	27
2.2	Convergence Analysis of the discontinuous Galerkin method applied to the cantilever beam problem in large deformation. The error in tip deflection $E v/s$ mesh size $h$ for $\beta = 1.5, 3, 15$ and the continuous Galerkin case . . . . .	28
2.3	Comparison of linear interpolation and quadratic interpolation for discontinuous Galerkin method for $beta = 1.515$ and continuous Galerkin method . . . . .	29
3.1	Schematic description of the Body $B_0$ , and the discretization $B_{0h}$ . . .	37
3.2	Interface Element with the two adjacent tetrahedra . . . . .	54
3.3	Data structure for Storing facet information . . . . .	55
4.1	Tensile test problem . . . . .	60

4.2	comparison of $u_z$ along $z$ axis of mesh 1 in 4.4 subjected to an tensile load and the analytical solution for the unidimensional tensile load problem . . . . .	61
4.3	Bi-material tensile loading test . . . . .	62
4.4	Tensile test problem discretization employed (a) mesh 1 ;(b) mesh 2; (c) mesh 3; (d) mesh 4. . . . .	63
4.5	Displacement profile for a bi material specimen subjected to tensile load	64
4.6	Strain profile for a bi material specimen subjected to tensile load . . .	64
4.7	Convergence analysis: $L^2$ norm of the displacement error v/s mesh size	65
4.8	Comparison of numerical and analytical results of strain profile along the $z$ axis for three different values of $\frac{l}{L}$ . . . . .	66
4.9	Bending problem illustration . . . . .	67
4.10	Plot of stiffness ratio to the ratio of length of the beam to the length scale parameter . . . . .	68
4.11	Description of the problem setup for torsional loading of a prismatic beam of square cross-section . . . . .	70
4.12	An illustration of the mesh used in the torsion example . . . . .	71
4.13	Plot of torsion stiffness ratio $\gamma$ to the ratio of thickness of the beam to the length scale parameter . . . . .	71
E.1	Comparison of strain profile in the domain for the the variation of $\frac{l}{L}$	103

# List of Tables

2.1	Geometric and material properties for beam bending problem . . . .	26
4.1	Tensile test material properties . . . . .	61
4.2	Bi-material tensile test material properties . . . . .	62
4.3	Bending test material properties . . . . .	67
4.4	Torsion test geometric and material properties . . . . .	69



# Chapter 1

## Introduction

A number of constitutive theories have arisen describing materials which, by nature, exhibit a non-local response. As-in, the stress at a material point is not just a function of strain at that particular point, as assumed in conventional theories, but also a function of strain in its local neighborhood, leading to the name *non local* or *strain gradient* theories. Cosserat, first proposed the couple stress theory , where in addition to the displacement  $u$  an independent rotation quantity  $\theta$  is also defined. The couple stresses are then introduced as the work conjugate of spatial gradient of  $\theta$ . Later Toupin [29] and Mindlin [30, 20] proposed a general theory theory which took into account not only micro-curvature but also gradients of normal strain. The initial theories proposed were for linear elastic materials. Later, several theories have been developed to take into account plastic flow theories (Fleck and Hutchinson[10, 22], Anand *et al.* [17]), crystal plasticity, crack growth (Smyshlyaev [38]) and several other microscopic behaviors exhibited by materials [19, 39, 37].

The formulation of boundary value problems, in the presence of higher order

gradients, leads to a system of equations involving higher-order derivatives which, in turn, makes the problem hard to solve both analytically and computationally. Computational difficulties arises in the solution scheme owing to the presence of higher order derivatives which in-turn require the solution field to be at least  $C^1$  continuity over the solution domain i.e. both the displacements and the first order derivatives should be continuous along the inter-element interface.

Zienkiewicz and Taylor [28] introduced a  $C^1$  continuous element, but its shape and the number of degrees of freedom needed per element puts serious limitations on its usability and scalability. A mixed type elements have been previously proposed, where at each node apart from the displacements an extra rotation angle  $\theta$  [41, 15, 16] or the couple stress is stored as nodal DOF. More recently, meshless Galerkin methods has been applied to problems with strain gradient effects in two dimensions.[14, 35]. Standard patch tests and benchmark problems have been tested on some of these methods, but rigorous mathematical proofs of rate of convergence, consistency and stability have not been demonstrated.

Discontinuous Galerkin methods are particularly attractive toward this end, as they provide a means to naturally and in a consistent way to enforce higher order inter-element continuity in a weak manner. Discontinuous Galerkin methods where first developed to solve neutron transport problem [33], has now been successfully applied to solve numerous elliptic and hyperbolic problems occurring in fluids and solid mechanics.[2, 8, 6, 36, 25, 27, 18]

In the context of elliptical problems Brezzi *et al.* [6] proposed a discontinuous galerkin method to solve the scalar poisson equation. Arnold *et al.* [1] presented a

detailed study of DG methods for second order elliptic equations. With the context of higher order elliptic equations Engel *et al.* [8] proposed the continuous-discontinuous(C/DG) Galerkin method, where the displacements across element interfaces are continuous whereas the jump in derivatives are penalized to impose  $C^1$  continuity across the elemental interface. They proposed a C/DG formulation and implementation in one dimensions for Bernoulli-Euler beam bending and Toupin-Mindlin strain gradient theory, and a formulation and implementation in two-dimension for poisson-kirchoffs plate theory. This sparked several related work toward's development of discontinuous galerkin methods for plate,shell theory problems and damage problems [40, 21]. Discontinuous Galerkin method has been developed for Reissner-Mindlin plates [2], Timoshenko beams [7], shells [12, 11] and for Kirchoff-Love shells [24]. Susanne *et al.* [4] developed rigorous stability and convergence results for a continuous-discontinuous galerkin method motivated from Engel *et al.* [8] toward's solving scalar fourth order elliptic equations in two-dimensions.

In this work, a discontinuous Galerkin formulation for boundary value problems in small strain, non-local linear elasticity is proposed. The underlying theory corresponds to the phenomenological strain-gradient theory developed by Fleck and Hutchinson [10] within the Toupin-Mindlin framework. The single-field displacement method obtained enables the discretization of the boundary value problem with a conventional continuous interpolation inside each finite element, whereas the higher-order inter element continuity is enforced in a weak manner. The proposed method is shown to be consistent and stable both theoretically and with suitable numerical examples.

In Chapter 2, the formulation and numerical examples of discontinuous Galerkin method for finite hyperelasticity with emphasis on alleviating the problem of locking which arises in low order finite element interpolation schemes. In Chapter 3, the formulation, analytical properties and finite element implementation of discontinuous Galerkin method for nonlocal linear elasticity is presented and to conclude in Chapter 4 results, conclusions and recommendation for future work are made.



# Chapter 2

## A low order discontinuous Galerkin method for finite hyperelasticity

### 2.1 Motivation

It is well established numerically and analytically that a higher order scheme have a better convergence rate when compared to lower order schemes [28]. However the advantage of a low order scheme is that it is relatively less expensive than the higher order schemes. Elements which employ linear interpolation are by far the most used and computationally an inexpensive method to get an approximate solution. When it comes to modeling incompressible materials and plasticity, finite element method exhibits locking [13]. In a conventional finite element method, this leads to decrease in convergence rate. It is also well established that the effects of locking are more prominent in linear elements in comparison to quadratic elements [13]. Several methods have been proposed to alleviate the problem of locking including mixed formu-

lation [9, 34], under integration [28] and they work very well. In this work we try to demonstrate one of the several advantages of employing a discontinuous Galerkin formulation developed for non-linear elasticity [25] intrinsically avoids the problem of locking. We choose a linear tetrahedral element, so as to clearly demonstrate that a discontinuous Galerkin formulation clearly eliminates locking. Firstly, we develop the discontinuous Galerkin formulation based on the work of Noels *et al.* [25, 26], where the discontinuous galerkin formulation is derived from the *weak form*, secondly discuss some of the implementation issues and finally numerical examples are presented towards this end.

## 2.2 Discontinuous Galerkin formulation

The governing equations along with the boundary conditions for a large static deformations of elastic bodies in equilibrium is given by,

$$\nabla_0 \mathbf{P} + \rho_0 \mathbf{B} = \mathbf{0} \text{ in } B_0 \quad (2.1)$$

$$\boldsymbol{\varphi} = \bar{\boldsymbol{\varphi}} \text{ on } \partial_D B_0 \quad (2.2)$$

$$\mathbf{P} \cdot \mathbf{N} = \bar{\mathbf{T}} \text{ on } \partial_N B_0 \quad (2.3)$$

where,  $B_0 \subset \mathbb{R}^3$  is the region occupied by the body in its reference configuration,  $\mathbf{P}$  is the first Piola-Kirchhoff stress tensor,  $\rho_0 \mathbf{B}$  represents body forces per unit reference volume,  $\nabla_0$  is the gradient operator in the reference frame,  $\boldsymbol{\varphi}$  is the corresponding deformation mapping of the deformation of material particles,  $\mathbf{N}$  is the unit normal

to the surface in the reference configuration and  $\bar{\boldsymbol{\varphi}}$  and  $\bar{\mathbf{T}}$  are the boundary conditions applied on the displacement  $\partial_D B_0$  and traction  $\partial_N B_0$  parts of the boundary, respectively. Also, its worthing noting that,  $\partial B_0 = \partial_D B_0 \cup \partial_N B_0$  and  $\partial_D B_0 \cap \partial_N B_0 = \emptyset$

For the constitutive law a general class of hyperelastic material models are considered for which stress can be computed from a strain energy density function  $W = W(\mathbf{F})$  given by:

$$\mathbf{P} = \frac{\partial W}{\partial \mathbf{F}} \quad (2.4)$$

where,  $\mathbf{F} = \nabla_0 \boldsymbol{\varphi}$  is the deformation gradients. As a direct consequence of Material frame indifference it can be easily shown that the strain energy density function  $W$  depends only on the right Cauchy-Green deformation tensor, that is  $W = W(\mathbf{C})$  and where  $\mathbf{C}$  is given by  $\mathbf{F}^T \mathbf{F}$ .

The first step towards the development of a discontinuous Galerkin formulation is discretization of the  $B_0$  into smaller domains  $\Omega_0^e$  such that

$$B_0 \approx B_{0h} = \bigcup_{e=1}^E \Omega_0^e \quad (2.5)$$

Here  $E$  is the total number of sub-domains present in the body,  $e$  is an index which runs over all the elements and  $B_{0h}$  an approximation for  $B_0$  represents the the body the union of  $\Omega_0^e$  represent. Since mesh generation, inter element interpolation and integration schemes are well developed for conventional finite element meshes (Tetrahedral & Hexahedral in 3-d), we are going to consider a decomposition of  $B_0$  into tetrahedral elements ( $\Omega_0^e$ ) for implementation purposes. But the mathematical

formulation presented in this section will hold good for any type of domain decomposition. Let subscript  $I$  correspond to the boundary between two sub-domains. Then  $\partial\Omega_0^e = \partial_D\Omega_0^e \cup \partial_N\Omega_0^e \cup \partial_I\Omega_0^e$  and  $\partial_I B_{0h} = \left[ \bigcup_{e=1}^E \partial\Omega_0^e \right]_{\setminus \partial B_{0h}}$ . Once the domain has been decomposed, the appropriate spaces for the test and trial functions have to be chosen in order to construct the solution. In a discontinuous Galerkin method we allow for discontinuities in the solution space along the internal surfaces ( $\partial_I B_{0h}$ ). That is, the field variables and the test function can have a jump along the interface of any two elements. Now, like in any finite element formulation it is essential to introduce a finite-dimensional piecewise polynomial approximation  $\varphi_h, \delta\varphi_h$  for the displacement field  $\varphi$  and test function  $\delta\varphi$  at all points inside the body  $B_{0h}$  which exist in the following spaces:

$$\mathbf{X}_h^k = \left\{ \varphi_h \in L^2(B_{0h}) \mid [\varphi_h|_{\Omega_0^e} \in \mathbb{P}^k(\Omega_0^e) \quad \forall \Omega_0^e \in B_{0h}] \right\} \quad (2.6)$$

$$\text{with } \mathbf{X}_{hc}^k = \left\{ \delta\varphi_h \in \mathbf{X}_h^k \mid [\delta\varphi_h|_{\partial_D B_{0h}} = 0] \right\} \quad (2.7)$$

The weak form of equilibrium equation (2.1) is obtained by multiplying equation with a test function ( $\delta\varphi_h$ ), and integrating in the domain ( $B_{0h}$ ).

$$\sum_e^E \int_{\Omega_0^e} \delta\varphi_h \nabla_0 \mathbf{P}_h dV_0 + \sum_e^E \int_{\Omega_0^e} \delta\varphi_h \rho_0 \mathbf{B} dV_0 = \mathbf{0} \quad \forall \delta\varphi \in \mathbf{X}_{hc}^k \quad (2.8)$$

Integrating the first term of equation(2.8) by parts

$$\begin{aligned} \mathbf{0} = & - \sum_e^E \int_{\Omega_0^e} \mathbf{P}_h : \nabla_0 \delta \varphi_h dV_0 + \sum_e^E \int_{\partial \Omega_0^e} \delta \varphi_h \cdot \mathbf{P}_h \cdot \mathbf{N} dS_0 \\ & + \sum_e^E \int_{\Omega_0^e} \delta \varphi_h \rho_0 \mathbf{B} dV_0 \quad \forall \delta \varphi \in X_{\text{hc}}^k \end{aligned} \quad (2.9)$$

We now separate the internal boundary terms( $\partial_I \Omega_0^e$ ) and the external boundary terms( $\partial_D \Omega_0^e \cup \partial_N \Omega_0^e$ ) in (2.9) using Neuman boundary condition (2.3) and from the definition of the test function space  $X_{\text{hc}}^k$  (2.7) leading to-

$$\begin{aligned} \mathbf{0} = & - \sum_e^E \int_{\Omega_0^e} \mathbf{P}_h : \nabla_0 \delta \varphi_h dV_0 + \sum_e^E \int_{\partial \Omega_0^e \cap \partial_I B_{0h}} \delta \varphi_h \cdot \mathbf{P}_h \cdot \mathbf{N} dS_0 \\ & + \sum_e^E \int_{\partial \Omega_0^e \cap \partial_N B_0} \delta \varphi_h \cdot \bar{\mathbf{T}} dS_0 + \sum_e^E \int_{\Omega_0^e} \delta \varphi_h \rho_0 \mathbf{B} dV_0 \quad \forall \delta \varphi \in X_{\text{hc}}^k \end{aligned} \quad (2.10)$$

It is appropriate to introduce the jump  $[[\bullet]]$  and the mean  $\langle \bullet \rangle$  operators defined on the space of functions which can have multiple values on the interior boundary  $\text{TR}(\partial_I B_{0h}) = \prod_{e=1}^E (L^2(\partial_I \Omega_0^e))$ :

$$[[\bullet]], \langle \bullet \rangle : [\text{TR}(\partial_I B_{0h})]^{1 \text{ or } 2} \rightarrow [L^2(\partial_I B_{0h})]^{1 \text{ or } 2} : [[\bullet]] = \bullet^+ - \bullet^-, \langle \bullet \rangle = \frac{1}{2} [\bullet^+ + \bullet^-] \quad (2.11)$$

In above expressions, the bullet represents any field,

$$\bullet^\pm = \lim_{\varepsilon \rightarrow 0^+} \bullet(\mathbf{X} \pm \varepsilon \mathbf{N}^-) \quad \forall \mathbf{X} \in \partial_I B_{0h} \quad (2.12)$$

and  $\mathbf{N}^-$  is the outward normal of  $\partial \Omega_0^e$ . The primary idea of discontinuous Galerkin

method is that, we allow for discontinuity on  $\mathbf{P}_h$  and  $\delta\varphi_h$  along the elemental interface  $\partial_I B_{h0}$ . The discontinuity along internal element interface is written as a flux term [26].

$$\sum_e^E \int_{\partial\Omega_0^e \cap \partial_I B_{0h}} \delta\varphi_h \cdot \mathbf{P}_h \cdot \mathbf{N} dS_0 \rightarrow - \int_{\partial_I B_{0h}} [[\delta\varphi_h]] \cdot \mathbf{h}(\mathbf{P}_h^-, \mathbf{P}_h^+, \mathbf{N}^-) dS_0 \quad (2.13)$$

where,  $\mathbf{h}(\mathbf{P}_h^-, \mathbf{P}_h^+, \mathbf{N}^-)$  is the inter-element flux term. Although we have an option in choosing any arbitrary flux term, in order to satisfy consistency of the weak formulation the flux should atleast satisfy the following properties [26].

$$\mathbf{h}(\mathbf{P}, \mathbf{P}, \mathbf{N}) = \mathbf{P} \cdot \mathbf{N} \quad (2.14)$$

$$\mathbf{h}(\mathbf{P}_h^-, \mathbf{P}_h^+, \mathbf{N}^-) = -\mathbf{h}(\mathbf{P}_h^+, \mathbf{P}_h^-, \mathbf{N}^+) \quad (2.15)$$

Using equation(2.13), equation (2.10) can be expressed as:

$$\begin{aligned} \mathbf{0} = & - \sum_e^E \int_{\Omega_0^e} \mathbf{P}_h : \nabla_0 \delta\varphi_h dV_0 - \int_{\partial_I B_{0h}} [[\delta\varphi_h]] \cdot \mathbf{h}(\mathbf{P}_h^-, \mathbf{P}_h^+, \mathbf{N}^-) dS_0 \\ & + \sum_e^E \int_{\partial\Omega_0^e \cap \partial_N B_0} \delta\varphi_h \cdot \bar{\mathbf{T}} dS_0 + \sum_e^E \int_{\Omega_0^e} \delta\varphi_h \rho_0 \mathbf{B} dV_0 \quad \forall \delta\varphi \in X_{hc}^k \end{aligned} \quad (2.16)$$

The stability of the weak form depends on the choice of flux. A wide repertoire of fluxes have been listed and their stability and convergence issues have been discussed by Arnold *et al.* [1]. For the following choice of flux, stability of the weak form has

been numerically and analytically demonstrated by Noels et al. [25]

$$\mathbf{h}(\mathbf{P}_h^-, \mathbf{P}_h^+, \mathbf{N}^-) = \langle \mathbf{P}_h \rangle \cdot \mathbf{N}^- + \mathbf{I} \otimes \mathbf{N}^- \cdot \left\langle \frac{\beta}{h_s} \bar{\mathbf{C}} \right\rangle \cdot [[\boldsymbol{\varphi}_h]] \otimes \mathbf{N}^- \quad (2.17)$$

where  $\bar{\mathbf{C}}$  is the mean tangent stiffness at the interface,  $\beta$  is an appropriate stability parameter chosen such that the scheme is stable and  $h_s$  is the characteristic length of the mesh

$$h_s = \min \left( \frac{|\Omega_0^{e-}|}{|\partial\Omega_0^{e-}|}, \frac{|\Omega_0^{e+}|}{|\partial\Omega_0^{e+}|} \right) \quad (2.18)$$

substituting (2.17) into the weakform (2.16), we get

$$\begin{aligned} 0 = & \int_{B_{0h}} \bar{\mathbf{P}} : \nabla_0 \delta \boldsymbol{\varphi}_h dV_0 - \int_{\partial_N B_{0h}} \bar{\mathbf{T}} \cdot \delta \boldsymbol{\varphi}_h dS_0 \\ & + \int_{\partial_I B_{0h}} [[\delta \boldsymbol{\varphi}_h]] \cdot \langle \bar{\mathbf{P}} \rangle \cdot \mathbf{N}^- dS_0 + \int_{\partial_I B_{0h}} [[\delta \boldsymbol{\varphi}_h]] \otimes \mathbf{N}^- \cdot \left\langle \frac{\beta}{h_s} \bar{\mathbf{C}} \right\rangle \cdot [[\boldsymbol{\varphi}_h]] \otimes \mathbf{N}^- dS_0 \end{aligned} \quad (2.19)$$

This is the final form of the discontinuous Galerkin formulation for non-linear elasticity. The stability, consistency and convergence of the above formulation is shown in Noels *et al.* [25]. This formulation also exactly corresponds to what's known as the *Interior Penalty method*. We have essentially derived the same formulation using the idea of an inter-element flux [5], instead of going through a more rigorous derivation.

## 2.3 Finite Element Implementation

The weak form as obtained in equation (2.19) can be easily implemented with little effort into a regular finite element code. Essentially the first two terms in the right hand side of equation (2.19) correspond to the terms arising from a standard Galerkin formulation. In order to perform integration over the internal surface an interface element very similar in notion to the ones used in cohesive elements for fracture is introduced [25]. A Newton-Raphson based solution procedure is setup to solve the system of non-linear algebraic equations given by

$$\mathbf{f}^{int}(x) + \mathbf{f}^I(x) = \mathbf{f}^{ext}(x). \quad (2.20)$$

Here  $\mathbf{f}^{int}$  is the internal force contributions that come from each volume element and is expressed as

$$\mathbf{f}_a^{int} = \int_{\Omega_e} \bar{\mathbf{P}} \cdot \mathbf{N}_{a,\mathbf{x}} dV_0, \quad (2.21)$$

$\mathbf{f}^I(x)$  is the internal force contributions from the interface elements and is expressed as

$$\begin{aligned} \mathbf{f}_a^{I\pm} = & \pm \int_{\partial_I B_{0h}} \langle \bar{\mathbf{P}} \rangle \cdot \mathbf{N}^- N_a dS_0 \\ & \pm \int_{\partial_I B_{0h}} \left[ \left\langle \frac{\beta}{h_s} \bar{\mathbf{C}} \right\rangle : [\mathbf{x}_\delta] \otimes \mathbf{N}^- \right] \cdot \mathbf{N}^- N_a N_b dS_0 \end{aligned} \quad (2.22)$$

At each iteration a linearized form equation (2.20) is solved and the nodal displacements are updated. The linearization of the left hand side of equation (2.20) results



in the tangent stiffness matrix ( $\mathbf{K}^{i-1}$ ) given as .

$$K_{iakk} = -\frac{\partial (f_{ia}^{int} + f_{ia}^I)}{\partial x_{kb}} \quad (2.23)$$

Rewriting equation (2.20) using the tangent stiffness matrix we obtain the linearized balance equation and the update equation.

$$\mathbf{K}^{i-1} \Delta \mathbf{U}^i = \mathbf{f}_{ext} - (\mathbf{f}_{int}^{i-1} + \mathbf{f}_J^{i-1}) \quad (2.24)$$

$$\mathbf{U}^i = \mathbf{U}^{i-1} + \Delta \mathbf{U}^i \quad (2.25)$$

Finally, in order to solve equation (2.24) we must compute the tangent stiffness of the system. we only present the stiffness terms that arise from the interface terms, the volume term being straightforward. We first make an approximation of the stiffness matrix contribution arising from the internal interface terms. From (2.19) its clear that the forces depend on the stresses and the material moduli. Therefore the stiffness matrix involves all the degrees of freedom of the two adjacent tetrahedral. But for large values of  $\beta$  the displacement jumps are small, therefore the stiffness term arising from the stress term is going to be very small [25]. Using this approximation, the interface stiffness matrix is given as:

$$\mathbf{K}_{ab}^{\pm\pm}{}_{ij} = \frac{\partial \mathbf{f}_{ai}^{\pm}}{\partial \mathbf{x}_b^{\pm}{}_{j}} = \pm \int_{\partial_I B_{0h}} \left\langle \frac{\beta}{h_s} \bar{\mathbf{C}} \right\rangle_{iJjL} N_a \mathbf{N}_J^- N_b \mathbf{N}_L^- dS \quad (2.26)$$

with a plus sign for the combinations  $\xi + \mu+$  and  $\xi - \mu-$  and with a minus sign for other combinations. This approximation helps us to simplify the implementation but at the time the stability of the scheme is not affected [25].

## 2.4 Numerical Results

In this section we will demonstrate with the help of a beam bending problem that even a linear tetrahedral at nearly incompressible poisson's ratio does not exhibit locking. In this calculation the material model corresponds to a NeoHookean model extended to the compressible range. The strain energy density function given as follows

$$W = \left( \frac{\lambda}{2} \log J - \mu \right) \log J + \frac{\mu}{2} (I_1 - 3) \quad (2.27)$$

where  $\lambda$  and  $\mu$  are the material parameters,  $J = \det((\mathbf{F}))$  and  $I_1 = tr(\mathbf{C})$ . The material parameters and the geometric characteristics of the beam used in calculations are listed in Table (2.1). In order to study the stability and convergence of the method

Table 2.1: Geometric and material properties for beam bending problem

Properties	values
Length	$L = 1m$
Height	$h = 0.1m$
Initial Young modulus	$E_0 = 200GPa$
Initial Poisson ratio	$\nu_0 = 0.4999$

in the first example we consider a prismatic beam with uniform cross-section whose geometric and material properties are listed in Table 2.1. The beam is clamped rigidly at one end and a force of  $10kN$  applied at the other. Using classical beam theory

the tip deflection  $\delta = 4(L^3/h^4)(F/E_0)$  is computed to be 2mm. The error in the tip deflection between numerical solution and analytical is plotted as a function of mesh size for three different values of  $\beta$  and is compared with the continuous Galerkin case. The tip displacement error remains a constant in the continuous Galerkin case,

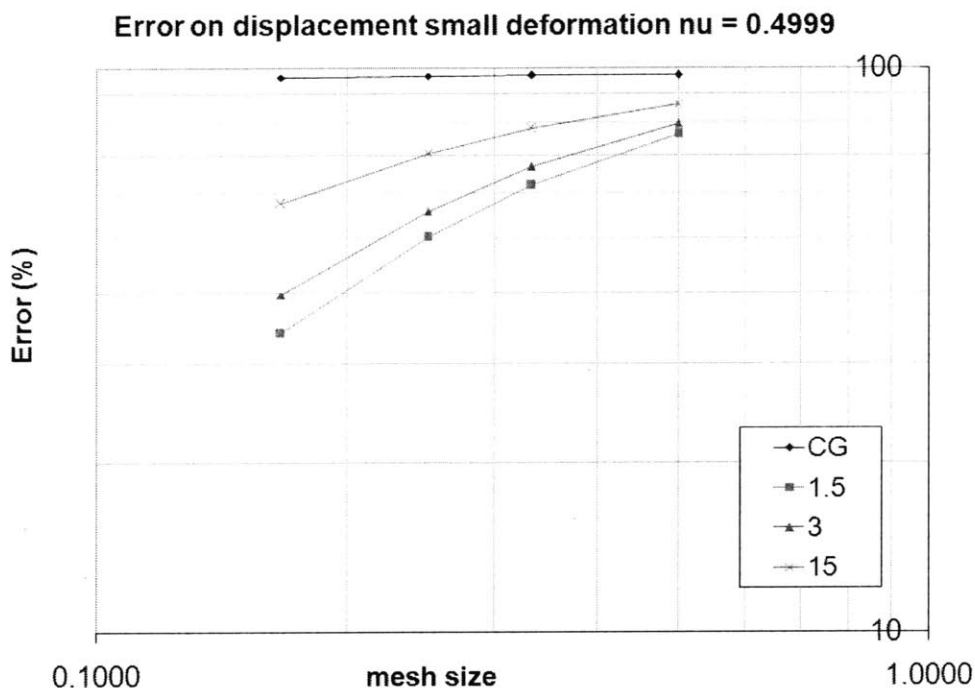


Figure 2.1: Convergence Analysis of the discontinuous Galerkin method applied to the cantilever beam problem in small deformation. The plot shows the error v/s mesh size  $h$  for  $\beta = 1.5, 3, 15$

whereas the error decreases with a slope equal to one for the discontinuous Galerkin formulation. The stabilization parameter  $\beta$  has no effect on the rate of convergence, but for a large value of  $\beta$ , the solution becomes less accurate and approaches the continuous Galerkin solution. The same convergence behavior is demonstrated for large deformations as well. To demonstrate the convergence behavior under large deformation's we consider use the same boundary value problem as described for

the small deformation bending problem but a load of  $1MN$  is applied on the right face, perpendicular to the length of the beam. In order to compute the error, we assume the fine mesh solution obtained using a quadratic element in a discontinuous Galerkin formulation to be the accurate solution and the error is computed with respect to this value. Figure (2.2) shows a very similar convergence pattern as to

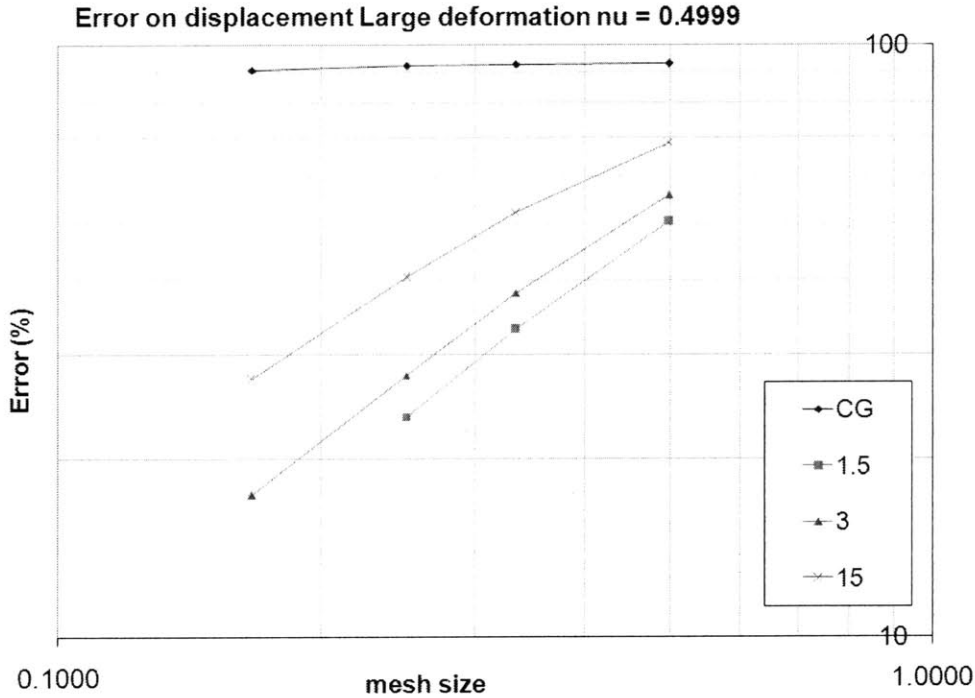


Figure 2.2: Convergence Analysis of the discontinuous Galerkin method applied to the cantilever beam problem in large deformation. The error in tip deflection  $E v/s$  mesh size  $h$  for  $\beta = 1.5, 3, 15$  and the continuous Galerkin case

the small deformation bending convergence. A comparison of the rate of convergence for linear and quadratic elements is studied for two different values of stabilization parameter  $\beta$  and for the continuous Galerkin formulation. From Figure (2.3) it is evident that for the same mesh size the quadratic elements have higher accuracy and

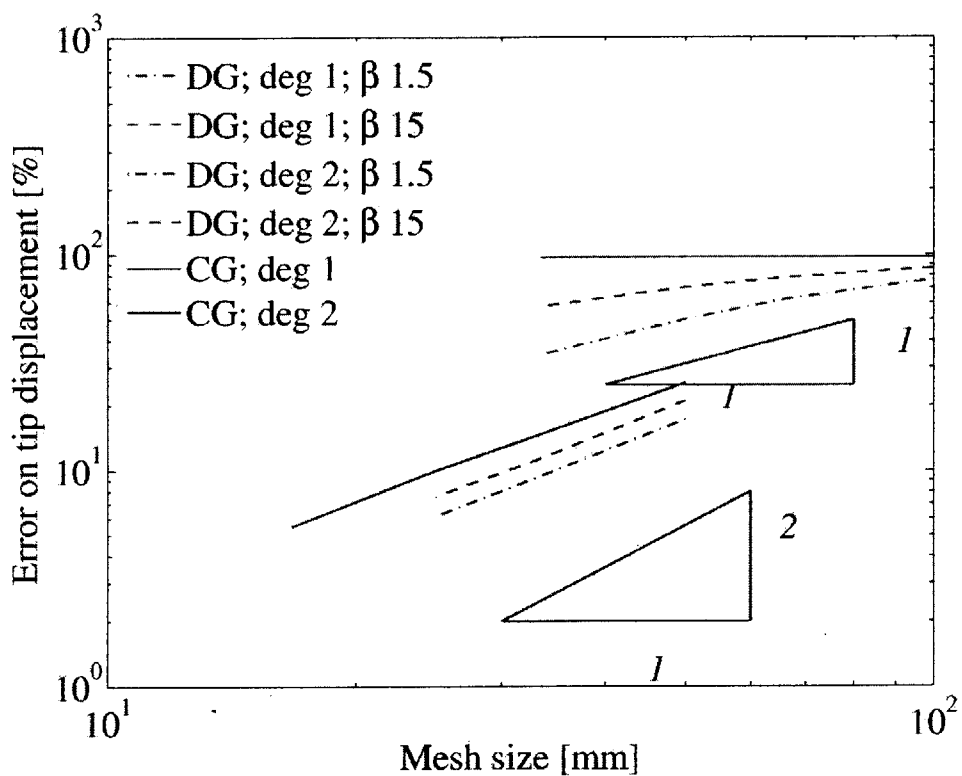


Figure 2.3: Comparison of linear interpolation and quadratic interpolation for discontinuous Galerkin method for  $\beta = 1.515$  and continuous Galerkin method

also the fact that the rate of convergence is higher for the quadratic elements when compared to the linear elements. To conclude, discontinuous Galerkin formulation does not exhibit locking and the convergence rate is not affected by Poisson's ratio.



# Chapter 3

## A discontinuous Galerkin formulation for linear nonlocal elasticity

### 3.1 Toupin-Mindlin strain-gradient theory of linear elasticity

In this section we present the linear elastic strain gradient theory developed by Toupin [29] and Mindlin [30]. In this theory the strain energy density function  $W$  per unit volume depends on the symmetric small strain measure  $\epsilon_{ij} = \frac{1}{2}(u_{i,j} + u_{j,i})$  and the higher order strain measure  $\eta_{ijk} = u_{k,ij}$ . The strain energy density is assumed be of

the form as given in equation (3.1)

$$W = W(\epsilon_{ij}, \eta_{ijk}) \quad (3.1)$$

The Cauchy stress  $\sigma_{ij}$  is the work conjugate of the strain measure  $\epsilon_{ij}$  whereas the higher order stress measure  $\tau_{ijk}$  is the work conjugate of the higher order strain measure  $\eta_{ijk}$  and following from (3.1)

$$\sigma_{ij} = \frac{\partial W}{\partial \epsilon_{ij}} \quad (3.2)$$

$$\tau_{ijk} = \frac{\partial W}{\partial \eta_{ijk}} \quad (3.3)$$

By employing the idea of virtual work the governing equations and the essential boundary conditions can be obtained in strong form [29, 30, 10]. Following the same procedure as shown by Fleck and Hutchinson [10], the internal virtual work statement can be written as

$$\begin{aligned} \int_{B_0} \delta W dV &= \int_{B_0} (\sigma_{ij} \delta \epsilon_{ij} + \tau_{ijk} \delta \eta_{ijk}) dV \\ &= \int_{B_0} \hat{b}_k \delta u_k dV + \int_{\partial_N B} \hat{t}_k \delta u_k dS + \int_{\partial_M B} \hat{r}_k \delta u_{k,l} n_l dS \end{aligned} \quad (3.4)$$

where,  $\partial_N B_0$  corresponds to the boundary where traction  $\hat{t}_k$  is specified,  $\partial_M B_0$  corresponds to the boundary where double stress traction  $\hat{r}_k$  is specified and  $\hat{b}_k$  is the body force acting per unit volume. Tractions  $\hat{t}_k$  and double stress traction  $\hat{r}_k$  are the nat-



ural boundary conditions of the problem and the corresponding essential boundary conditions are the displacement  $\hat{u}_k$  specified on the surface  $\partial_D B_0$  and the gradient of displacement projected along the normal to the surface  $n_i u_{k,i}$  on the surface  $\partial_T B_0$ . It is worth noting that  $\partial_N B_0 \cup \partial_D B_0 = \partial B_0$ ,  $\partial_N B_0 \cap \partial_D B_0 = \emptyset$ ,  $\partial_M B_0 \cup \partial_T B_0 = \partial B_0$  and  $\partial_M B_0 \cap \partial_T B_0 = \emptyset$ . A schematic description of the different boundary conditions is illustrated in figure (3.1). Applying Gauss divergence theorem to the internal work terms in equation (3.4), we obtain

$$\begin{aligned} \int_{B_0} (\sigma_{ij} \delta \epsilon_{ij} + \tau_{ijk} \delta \eta_{ijk}) dV = & - \int_{B_0} (\sigma_{ik} - \tau_{ijk,j})_i \delta u_k dV + \int_{\partial B_0} n_i (\sigma_{ik} - \tau_{ijk,j}) \delta u_k dS \\ & + \int_{\partial B_0} n_j \tau_{ijk} \delta u_{k,i} dS \end{aligned} \quad (3.5)$$

Here in equation(3.5),  $\partial B_0$  is the surface of the body,  $n_i$  is the unit normal to the surface of the body. However its worth noting that  $\delta u_k$  vanishes at all points on the surface  $\partial_D B_0$ , reducing equation (3.5) into

$$\begin{aligned} \int_{B_0} (\sigma_{ij} \delta \epsilon_{ij} + \tau_{ijk} \delta \eta_{ijk}) dV = & - \int_{B_0} (\sigma_{ik} - \tau_{ijk,j})_i \delta u_k dV + \int_{\partial_N B_0} n_i (\sigma_{ik} - \tau_{ijk,j}) \delta u_k dS \\ & + \int_{\partial B_0} n_j \tau_{ijk} \delta u_{k,i} dS \end{aligned} \quad (3.6)$$

It has to be noted that  $\delta u_{k,i}$  is not independent of  $\delta u_k$  on the surface( $\partial B_0$ ) of Body ( $B$ ) [10, 20]. So, in order to correctly identify the boundary conditions the gradient of the virtual applied displacement on the surface is split into two components, the

normal gradient component,  $n_i D\delta u_k$  and the surface gradient component,  $D_i\delta u_k$ .

$$\begin{aligned}\delta u_{k,i} &= (\delta_{il} - n_i n_l) (u_k)_{,l} + n_i n_l (u_k)_{,l} \\ &= D_i\delta u_k + n_i D\delta u_k\end{aligned}\tag{3.7}$$

substituting equation(3.7) in equation (3.5)

$$\begin{aligned}\int_{B_0} (\sigma_{ij}\delta\epsilon_{ij} + \tau_{ijk}\delta\eta_{ijk}) dV &= - \int_{B_0} (\sigma_{ik} - \tau_{ijk,j})_i \delta u_k dV + \int_{\partial_N B_0} n_i (\sigma_{ik} - \tau_{ijk,j}) \delta u_k dS \\ &+ \int_{\partial B_0} n_j \tau_{ijk} (\delta_{il} - n_i n_l) \delta u_{k,l} dS + \int_{\partial B_0} n_j \tau_{ijk} n_i n_l \delta u_{k,l} dS\end{aligned}\tag{3.8}$$

The surface gradient term on the right hand side of equation (3.8) can be further simplified using integration by parts<sup>1</sup> and followed by applying the surface divergence theorem<sup>2 3</sup>.

$$\begin{aligned}&\int_{\partial B_0} n_j \tau_{ijk} (\delta_{il} - n_i n_l) \delta u_{k,l} dS \\ &= \int_{\partial B_0} (\delta_{il} - n_i n_l) (n_j \tau_{ijk} \delta u_k)_{,l} dS - \int_{\partial B_0} (\delta_{il} - n_i n_l) (n_j \tau_{ijk})_{,l} \delta u_k dS \\ &= \int_{\partial B_0} (\delta_{lm} - n_l n_m) n_{l,m} (n_j n_i \tau_{ijk}) \delta u_k dS - \int_{\partial B_0} (\delta_{il} - n_i n_l) (n_j \tau_{ijk})_{,l} \delta u_k dS\end{aligned}\tag{3.9}$$

It should be noted in equation (3.9), that  $\delta u_k$  will vanish on the surface  $\partial_D B_0$  and in equation (3.8)  $\delta u_{k,l} n_l$  vanishes on  $\partial_T B_0$ , thus from equation (3.9) , the internal

---

<sup>1</sup> $\phi : \nabla^s v = \nabla^s \cdot (\phi \cdot v) - (\nabla^s \cdot \phi) \cdot v$  where  $\nabla^s$  is the surface gradient operator

<sup>2</sup> $\int_s \nabla^s \cdot (\phi \cdot v) dS = \int_s (\nabla_s \cdot n) n \cdot \phi \cdot v dS$  [30]

<sup>3</sup>It is noted here that the surface is assumed to be smooth and that there are no edges.

virtual work terms now become

$$\begin{aligned}
\int_{B_0} (\sigma_{ij} \delta \epsilon_{ij} + \tau_{ijk} \delta \eta_{ijk}) dV &= - \int_{B_0} (\sigma_{ik} - \tau_{ijk,j})_i \delta u_k dV + \int_{\partial_N B_0} n_i (\sigma_{ik} - \tau_{ijk,j}) \delta u_k dS \\
+ \int_{\partial_N B_0} (\delta_{lm} - n_l n_m) n_{l,m} (n_j n_i \tau_{ijk}) \delta u_k dS &- \int_{\partial_N B_0} (\delta_{il} - n_i n_l) (n_j \tau_{ijk})_{,l} \delta u_k dS \\
+ \int_{\partial_M B_0} n_j \tau_{ijk} n_i n_l \delta u_{k,l} dS &
\end{aligned} \tag{3.10}$$

using equation (3.10), the principle of virtual work equation (3.4), is satisfied if the following local conditions hold true:

$$0 = \hat{b}_k + (\sigma_{ik} - \tau_{ijk,j})_{,i} \tag{3.11}$$

which represents the governing differential equation in strong form

$$\hat{t}_k = n_i (\sigma_{ik} - \partial_j \tau_{ijk}) + n_i n_j \tau_{ijk} (D_p n_p) - D_i (n_j \tau_{ijk}) \tag{3.12}$$

is the traction boundary condition on the surface  $\partial_N B_0$  and

$$\hat{r}_k = n_i n_j \tau_{ijk} \tag{3.13}$$

is the applied double stress traction  $\hat{r}_k$  on  $\partial B_M$ . It is assumed that the body has a smooth surface  $\partial B_0$  so that there are no edges, since the presence of edges will result in an additional integral term over the edge [10]. The governing balance equation (3.11) can be uniquely solved along with the six boundary conditions in (3.11) and (3.13) if

the strain energy density function used is convex with respect to both  $\epsilon_{ij}$  and  $\eta_{ijk}$  [22]. The boundary value problem resulting from the virtual work statement correspond to the non local linear elastic theory proposed by Toupin [29] and Mindlin[30], which can be summarized as follows

$$0 = b_k + (\sigma_{ik} - \tau_{jik,j})_{,i} \text{ in } B_0 \quad (3.14)$$

$$\sigma_{ij} = \frac{\partial W}{\partial \epsilon_{ij}} \text{ in } B_0 \quad (3.15)$$

$$\tau_{ijk} = \frac{\partial W}{\partial \eta_{ijk}} \text{ in } B_0 \quad (3.16)$$

$$\epsilon_{ij} = \frac{1}{2} (u_{i,j} + u_{j,i}) \text{ in } B_0 \quad (3.17)$$

$$\eta_{ijk} = u_{k,ij} \text{ in } B_0 \quad (3.18)$$

$$\hat{t}_k = n_i (\sigma_{ik} - \partial_j \tau_{ijk}) + n_i n_j \tau_{ijk} (D_p n_p) - D_i (n_j \tau_{ijk}) \text{ on } \partial_N B_0 \quad (3.19)$$

$$\hat{r}_k = n_i n_j \tau_{ijk} \text{ on } \partial_M B_0 \quad (3.20)$$

$$u_k = \bar{u}_k \text{ on } \partial_D B_0 \quad (3.21)$$

$$n_i u_{k,i} = \overline{D u_{k,i}} \text{ on } \partial_T B_0 \quad (3.22)$$

In the next section we will develop the discontinuous Galerkin formulation for the boundary value problem described by equation (3.14, 3.19, 3.20 -3.22) and establish stability and convergence properties.

## 3.2 Discontinuous Galerkin formulation

The preceding formulation of the boundary value problem in strong form is taken as a basis for the formulation of a discontinuous Galerkin weak form approximation

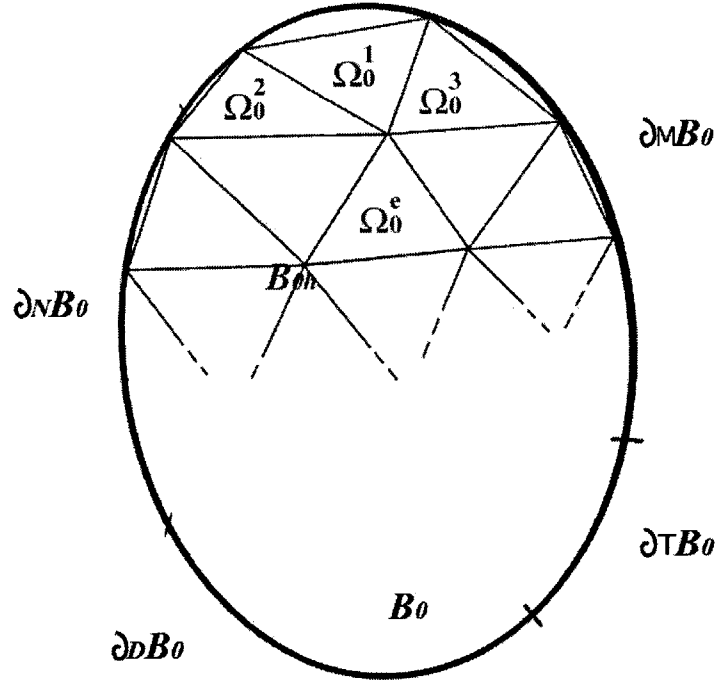


Figure 3.1: Schematic description of the Body  $B_0$ , and the discretization  $B_{0h}$

within the context of a finite element framework. The first step in the development of a discontinuous Galerkin formulation is the decomposition of the domain ( $B_0$ ) into smaller sub-domains ( $\Omega_e$ ) such that  $\bigcup_{e=1}^E \Omega_e = B_{0h} \approx B_0$ . As the mesh size ( $h$ ) is decreased, the body modeled by the meshes becomes closer to the actual geometry of the body. The next step is to define the spaces for the trial ( $u_k$ ) and the test functions ( $w_k$ ), which are  $C^0$  continuous

$$U_h^k = \left\{ \mathbf{u}_h \in C^0(B_{0h}) \subset \mathbf{L}^2(B_{0h}) \mid \mathbf{u}_h|_{\Omega_e} \in \mathbb{P}^k(\Omega_e^e) \quad \forall \Omega_e \in B_{0h} \right\} \subset U^f(B_{0h}) \quad (3.23)$$

Where  $U^f(B_{0h}) = \prod_e \mathbf{H}^2(\Omega_e)$  for  $k > 1$ . It should be clear that this choice of interpolation and trial spaces allow for  $C^1$  jump discontinuities at the internal boundaries

between elements  $\partial_I \Omega = [\cup_{e=1}^E \partial \Omega_e]_{\setminus \partial B_0}$ . The corresponding constrained space for the test function is

$$U_{hc}^k = \left\{ \delta \mathbf{u} \in U_h^k \mid \delta \mathbf{u} \big|_{\partial_U B_0} = 0 \right\} \subset U_c^f(B_0) \quad (3.24)$$

$$U_c^f = \left\{ \delta \mathbf{u} \in U^f \mid \delta \mathbf{u} \big|_{\partial_U B_0} = 0 \right\} \quad (3.25)$$

We start with the equilibrium equation (3.14) and multiply with a test function  $\mathbf{w} \in U_{hc}^f$  and impose equilibrium in a weak sense

$$\sum_{e=1}^E \int_{\Omega_e} w_k \left( b_k + (\sigma_{ik} - \tau_{jik,j})_{,i} \right) dV = 0 \quad \forall \mathbf{w} \in U_{hc}^f \quad (3.26)$$

From now on it will be assumed that the test functions belong to the constrained space (3.24). Applying integration by parts followed by Gauss divergence theorem

$$\begin{aligned} \sum_{e=1}^E \int_{\partial \Omega_e} w_k (\sigma_{ik} - \tau_{jik,j}) n_i dS - \sum_{e=1}^E \int_{\Omega_e} w_{k,i} \sigma_{ik} dV - \sum_{e=1}^E \int_{\Omega_e} w_{k,ij} \tau_{jik} dV \\ + \sum_{e=1}^E \int_{\partial \Omega_e} w_{k,i} \tau_{jik} n_j dS + \sum_{e=1}^E \int_{\Omega_e} w_k b_k dV = 0 \end{aligned} \quad (3.27)$$

The integrals over the boundary of each element ( $\partial \Omega_e$ ) can be written as a summation of integrals over the internal interfaces and a summation over the external boundaries

$$\begin{aligned}
& \sum_{e=1}^E \int_{\partial\Omega_e \cap \partial_I \Omega} w_k (\sigma_{ik} - \tau_{jik,j}) n_i dS - \sum_{e=1}^E \int_{\Omega_e} w_{k,i} \sigma_{ik} dV - \sum_{e=1}^E \int_{\Omega_e} w_{k,ij} \tau_{jik} dV \\
& + \sum_{e=1}^E \int_{\partial\Omega_e \cap \partial_I \Omega} w_{k,i} \tau_{jik} n_j dS + \sum_{e=1}^E \int_{\Omega_e} w_k b_k dV + \sum_{e=1}^E \int_{\partial\Omega_e \cap \partial\Omega} w_{k,i} \tau_{jik} n_j dS \quad (3.28) \\
& + \sum_{e=1}^E \int_{\partial\Omega_e \cap \partial\Omega} w_k (\sigma_{ik} - \tau_{jik,j}) n_i dS = 0
\end{aligned}$$

Now defining a jump operator  $\llbracket \bullet \rrbracket = \bullet^+ - \bullet^-$  and a mean operator  $\langle \bullet \rangle = \frac{1}{2} (\bullet^+ + \bullet^-)$ , the first term of equation (3.28) can be expanded as follows.

$$\begin{aligned}
\sum_{e=1}^E \int_{\partial\Omega_e \cap \partial_I \Omega} w_k (\sigma_{ik} - \tau_{jik,j}) n_i^- dS &= - \int_{\partial_I \Omega} (w_k^+ (\sigma_{ik} - \tau_{jik,j})^+ n_i^+ \\
& + w_k^- (\sigma_{ik} - \tau_{jik,j})^- n_i^-) dS \\
&= - \int_{\partial_I \Omega} \llbracket w_k (\sigma_{ik} - \tau_{jik,j}) \rrbracket n_i^- dS \quad (3.29) \\
&= - \int_{\partial_I \Omega} \llbracket w_k \rrbracket \langle \sigma_{ik} - \tau_{jik,j} \rangle n_i^- dS \\
& \quad - \int_{\partial_I \Omega} \langle w_k \rangle \llbracket \sigma_{ik} - \tau_{jik,j} \rrbracket n_i^- dS
\end{aligned}$$

where  $\bullet^\pm$  denotes quantities on either side of the interface element,  $n_k^-$  is the outward normal of the bottom tetrahedron. Here we have used the fact that on the interelement interface  $n^- = -n^+$ , the definition of the jump and mean operator and using the relation  $\llbracket ab \rrbracket = \llbracket a \rrbracket \langle b \rangle + \langle a \rangle \llbracket b \rrbracket$ . The last term in equation (3.29) can be neglected because only compatibility of displacements needs to be enforced. In the first term  $\llbracket w_k \rrbracket = 0$ , since the space of interpolation and trial functions are assumed to be  $C^0$  continuous in the whole domain (3.24). The second interelement boundary term in

equation (3.28) can be written as:

$$\begin{aligned}
\sum_{e=1}^E \int_{\partial\Omega_e \cap \partial_I\Omega} w_{k,i} \tau_{jik} n_j^- dS &= \int_{\partial_I\Omega} (w_{k,i}^+ \tau_{jik}^+ n_j^+ + w_{k,i}^- \tau_{jik}^- n_j^-) dS \\
&= - \int_{\partial_I\Omega} \llbracket w_{k,i} \tau_{jik} \rrbracket n_j dS \\
&= - \int_{\partial_I\Omega} \llbracket w_{k,i} \rrbracket \langle \tau_{jik} \rangle n_j^- dS - \int_{\partial_I\Omega} \langle w_{k,i} \rangle \llbracket \tau_{jik} \rrbracket n_j^- dS
\end{aligned} \tag{3.30}$$

The last term of equation (3.30) can be neglected because only compatibility of displacement gradients needs to be enforced. The mean higher order stress  $\langle \tau_{jik} \rangle$  can be expressed as a flux term  $\widehat{\tau_{jik} n_j^-}$  following the work of Brezzi et al. [5, 6], Arnold et al. [1], Noels et al [26].

$$\sum_{e=1}^E \int_{\partial\Omega_e \cap \partial_I\Omega} w_{k,i} \tau_{jik} n_j dS \approx - \int_{\partial_I\Omega} \llbracket w_{k,i} \rrbracket \widehat{\tau_{jik} n_j^-} dS \tag{3.31}$$

Inserting equation (3.29), (3.30), (3.31) into equation (3.28) we obtain

$$\begin{aligned}
&\sum_e \int_{\Omega_e} w_{k,i} \sigma_{ik} d\Omega + \sum_e \int_{\Omega_e} w_{k,ij} \tau_{jik} d\Omega + \int_{\partial_I\Omega} \llbracket w_{k,i} \rrbracket \widehat{\tau_{jik} n_j} dS \\
&- \int_{\partial\Omega} w_k (\sigma_{ik} - \tau_{jik,j}) n_i dS \\
&- \int_{\partial\Omega} w_{k,i} (\tau_{jik} n_j) dS - \sum_e \int_{\Omega_e} w_k b_k d\Omega = 0.
\end{aligned} \tag{3.32}$$

For the sake of convenience the superscript on the normal is dropped, but it should be noted that when we refer to the normal of an internal surface, it corresponds to the outward normal of the oriented interelement boundary surface. Following the



procedure established in the previous section, the boundary integral terms occurring on the boundary  $\partial\Omega$  in equation (3.32) can be written as.

$$\begin{aligned}
& \int_{\partial\Omega} w_{k,i} (\tau_{jik} n_j) dS + \int_{\partial\Omega} w_k (\sigma_{ik} - \tau_{jik,j}) n_i dS \\
&= \int_{\partial\Omega} w_k [n_i n_j \tau_{ijk} (D_p n_p) - D_j (n_i \tau_{ijk}) + (\sigma_{ik} - \tau_{jik,j}) n_i] d\Omega \quad (3.33) \\
&+ \int_{\partial\Omega} n_i \tau_{jik} n_j w_{k,l} n_l d\Omega
\end{aligned}$$

From the first term in the right hand side of the first term in equation (3.33),  $\int_{\partial\Omega} w_k (n_i n_j \tau_{ijk} (D_p n_p) - D_j (n_i \tau_{ijk}) + (\sigma_{ik} - \tau_{jik,j}) n_i) d\Omega$  constitutes the weak enforcement of the traction boundary condition  $\hat{t}_k$ . The conjugate of this traction condition is the displacement (Dirichlet) condition. Since the displacement boundary condition can be enforced strongly, this term reduces to an integral over the Neumann boundary ( $\partial_N B_0$ ). The second term in the right hand side of equation (3.33)  $\int_{\partial\Omega} n_i \tau_{jik} n_j w_{k,l} n_l d\Omega$  constitutes the weak enforcement of the higher order traction boundary condition  $\hat{r}_k$  and its conjugate boundary condition is the normal component of the displacement gradient ( $n_j u_{i,j} = \overline{D u_i}$ ) on the surface. In the single field displacement method proposed, displacement gradient cannot be specified independently and therefore higher order Dirichlet boundary condition need to be enforced weakly. Which is equivalent of imposing a boundary flux term  $\widehat{\tau_{jik} n_j}$  on  $\partial_T B_0$ . It is also worth noting that the internal surface flux term and the external surface flux term are very similar in form.

The boundary terms now are given by

$$\begin{aligned}
& \int_{\partial\Omega} w_{k,i} (\tau_{jik} n_j) dS + \int_{\partial\Omega} w_k (\sigma_{ik} - \tau_{jik,j}) n_i dS \\
&= \int_{\partial_N\Omega} w_k (n_i n_j \tau_{ijk} (D_p n_p) - D_j (n_i \tau_{ijk}) + (\sigma_{ik} - \tau_{jik,j}) n_i) d\Omega \\
&+ \int_{\partial_T\Omega} n_i w_{k,l} n_l \widehat{\tau_{jik} n_j} d\Omega + \int_{\partial_M\Omega} \hat{r}_k w_{k,l} n_l d\Omega \\
&= \int_{\partial_N\Omega} w_k \hat{t}_k d\Omega + \int_{\partial_T\Omega} n_i w_{k,l} n_l \widehat{\tau_{jik} n_j} d\Omega + \int_{\partial_M\Omega} \hat{r}_k w_{k,l} n_l d\Omega
\end{aligned} \tag{3.34}$$

Substituting equation (3.34) into the weak form we obtain

$$\begin{aligned}
& \sum_e \int_{\Omega_e} w_{k,i} \sigma_{ik} d\Omega + \sum_e \int_{\Omega_e} w_{k,i,j} \tau_{jik} d\Omega + \int_{\partial_I\Omega} [[w_{k,i}]] \widehat{\tau_{jik} n_j} dS \\
&- \int_{\partial_N\Omega} w_k t_k dS - \int_{\partial_T\Omega} n_i w_{k,l} n_l \widehat{\tau_{jik} n_j} d\Omega - \int_{\partial_M\Omega} \hat{r}_k w_{k,l} n_l d\Omega \\
&- \sum_e \int_{\Omega_e} w_k b_k d\Omega = 0
\end{aligned} \tag{3.35}$$

We will now direct attention towards the definition of the flux term in the discontinuous Galerkin formulation. The flux term will be defined such that the discontinuous Galerkin formulation is consistent and stable. Following [25], first we define the numerical flux on the internal surface  $\partial_I\Omega$  as

$$\widehat{\tau_{jik} n_j} = \langle \tau_{jik} \rangle n_j + n_j \left\langle \frac{\beta J_{jikqrp}}{h} \right\rangle [[u_{p,q}]] n_r \tag{3.36}$$

where  $\beta$  is a stabilization parameter and  $h$  is the characteristic length of the mesh.

$$h = \min \left( \frac{|\Omega_0^{e-}|}{|\partial\Omega_0^{e-}|}, \frac{|\Omega_0^{e+}|}{|\partial\Omega_0^{e+}|} \right) \tag{3.37}$$

The flux term on the external boundary  $\partial_T\Omega$  is given as

$$\widehat{\tau_{jik}n_j} = \tau_{jik}n_j + n_j \frac{\beta J_{jikqrp}}{h} (n_s u_{p,s} n_q - \overline{Du_p} n_q) n_r \quad (3.38)$$

and  $h$  on the external boundary of the mesh is given by

$$h = \frac{|\Omega_0^e|}{|\partial\Omega_0^e|} \quad (3.39)$$

here  $\overline{Du_p}$  is the externally specified normal component of the displacement gradient. It is interesting to note that the idea of imposing boundary conditions in a weak sense was introduced by [23]. This flux term is similar in notion to the average flux introduced by Bassi and Rebay [3] for fluids and the stabilization term is of the quadratic type. Inserting the specific form of the flux term into the equilibrium equation we obtain the stable discontinuous Galerkin formulation for nonlocal linear elasticity

$$\begin{aligned} 0 &= \sum_e \int_{\Omega_e} w_{k,i} \sigma_{ik} d\Omega + \sum_e \int_{\Omega_e} w_{k,ij} \tau_{jik} d\Omega - \int_{\partial_N\Omega} w_k \hat{t}_k dS - \sum_e \int_{\Omega_e} w_k b_k d\Omega \\ &+ \int_{\partial_T\Omega} \llbracket w_{k,i} \rrbracket \left[ \langle \tau_{jik} \rangle n_j + n_j \left\langle \frac{\beta J_{jikqrp}}{h} \right\rangle \llbracket u_{p,q} \rrbracket n_r \right] dS - \int_{\partial_M\Omega} w_{k,l} n_l \hat{r}_k dS \\ &- \int_{\partial_T\Omega} w_{k,l} n_l n_i \left[ \tau_{jik} n_j + n_j \frac{\beta J_{jikqrp}}{h} (n_s u_{p,s} n_q - \overline{Du_p} n_q) n_r \right] dS \\ \forall w_k &\in U_{hc}^f \end{aligned} \quad (3.40)$$

Equation (3.40) is the final weak form of the nonlocal linear elasticity problem along with the Dirichlet boundary condition  $u_i = \bar{u}_i$  on  $\partial_D B_0$  which is enforced strongly. In the next section, the theoretical stability and convergence properties of the discon-

tinuous Galerkin method will be demonstrated.

### 3.3 Theoretical stability and convergence

In this section we will demonstrate that the discontinuous Galerkin formulation for non local elasticity has the necessary properties essential for numerical convergence. The consistency and the stability of the method as well as the convergence rate are demonstrated.

#### 3.3.1 Consistency

Let us consider the exact solution to the physical problem  $u \in \mathbf{H}^2(B_{h0})$ . In particular, this solution belongs to  $\mathbf{C}^1(B_{h0})$ , therefore one has the following properties-

$$\llbracket u_{i,j} \rrbracket = 0 \quad \text{on } \partial_I B_0 \tag{3.41}$$

$$\eta_{ijk} = u_{k,ij} \quad \text{in } B_0 \tag{3.42}$$

$$\langle \tau_{ijk} \rangle = \tau_{ijk} \quad \text{in } B_0 \tag{3.43}$$

Applying Gauss divergence theorem to equation (3.40) and using equations (3.41, 3.42, 3.43 we obtain-

$$\begin{aligned}
& \int_{B_{0h}} w_k b_k d\Omega + \int_{\partial_N \Omega} w_k \hat{t}_k dS + \int_{\partial_M \Omega} w_{k,l} n_l \hat{r}_k dS + \int_{\partial_T \Omega} w_{k,l} n_l n_j n_i \frac{\beta J_{jikqrp}}{h} n_s \hat{u}_{p,s} n_q n_r dS \\
&= \int_{\partial_N \Omega} w_k \sigma_{ik} n_i dS - \int_{B_{0h}} w_k \sigma_{ik,i} d\Omega + \int_{\partial \Omega} w_{k,i} \tau_{jik} n_j dS - \int_{\partial \Omega} w_k \tau_{jik,j} n_i dS \\
&- \int_{\partial_I \Omega} \llbracket w_{k,i} \rrbracket \langle \tau_{jik} \rangle n_j dS + \int_{B_{0h}} w_{k,ij} \tau_{jik} d\Omega + \int_{\partial_I \Omega} \llbracket w_{k,i} \rrbracket \langle \tau_{jik} \rangle n_j dS \\
&+ \int_{\partial_T \Omega} w_{k,l} n_l n_i n_j \frac{\beta J_{jikqrp}}{h} n_s u_{p,s} n_q n_r dS
\end{aligned} \tag{3.44}$$

In the above expression, canceling the interelement jump term, decomposing the boundary terms in the right hand side into mutually independent conditions as we did in the previous section and taking into account the spaces to which the test functions belong, we obtain

$$\begin{aligned}
& \int_{B_{0h}} w_k b_k d\Omega + \int_{\partial_N \Omega} w_k (t_k - \hat{t}_k) dS + \int_{\partial_M \Omega} w_{k,l} n_l (r_k - \hat{r}_k) dS \\
&+ \int_{\partial_T \Omega} w_{k,l} n_l n_i n_j \frac{\beta J_{jikqrp}}{h} (n_s u_{p,s} n_q - n_s \hat{u}_{p,s} n_q) n_r dS \\
&= - \int_{B_{0h}} w_k \sigma_{ik,i} d\Omega + \int_{B_{0h}} w_{k,ij} \tau_{jik} d\Omega
\end{aligned} \tag{3.45}$$

From the above equation it is clear that the strong form of the equilibrium equation is recovered, thus showing the consistency of the scheme.

$$0 = b_k + (\sigma_{ik} - \tau_{jik,j})_{,i} \text{ in } B_{0h} \quad (3.46)$$

$$t_k = n_i (\sigma_{ik} - \partial_j \tau_{ijk}) + n_i n_j \tau_{ijk} (D_p n_p) - D_i (n_j \tau_{ijk}) \text{ on } \partial_N B_0 \quad (3.47)$$

$$r_k = n_i n_j \tau_{ijk} \quad (3.48)$$

$$n_s u_{p,s} = n_s \hat{u}_{p,s} \text{ on } \partial_M B_0 \quad (3.49)$$

consistency leads to orthogonality, As the formulation is consistent, the exact solution ( $\mathbf{u}$ ) will also satisfy equation (3.45), therefore we have

$$a(\mathbf{u}_h - \mathbf{u}, \delta \mathbf{u}) = a(\mathbf{u}_h, \delta \mathbf{u}) - a(\mathbf{u}, \delta \mathbf{u}) = a(\mathbf{u}_h, \delta \mathbf{u}) - b(\delta \mathbf{u}) = 0 \quad (3.50)$$

### 3.3.2 Stability

Before we proceed to analytically demonstrate the stability of the proposed numerical scheme it will be necessary to define an energy norm  $\|\cdot\| : U_c^f(B_0) \rightarrow \mathbb{R}_+$

$$\begin{aligned} \|\mathbf{v}\|^2 &= \sum_e \left\| \sqrt{C_{ijkl}} v_{k,l} \right\|_{L^2(\Omega^e)}^2 + \sum_e \left\| \sqrt{J_{ijklmn}} v_{n,lm} \right\|_{L^2(\Omega^e)}^2 \\ &+ \sum_e \frac{1}{2} \left\| \sqrt{\frac{J_{ijklmn}}{h}} \llbracket v_{n,l} \rrbracket n_m^- \right\|_{L^2(\partial\Omega^e \cap \partial_I B_h)}^2 \end{aligned} \quad (3.51)$$

with the abuse of notations

$$\sum_e \left\| \sqrt{C_{ijkl}} v_{k,l} \right\|_{L^2(\Omega^e)}^2 = \int_{B_h} v_{i,j} C_{ijkl} v_{k,l} d\Omega \quad (3.52)$$

$$\sum_e \left\| \sqrt{J_{ijklmn}} v_{n,lm} \right\|_{L^2(\Omega^e)}^2 = \int_{B_h} v_{k,ij} J_{ijklmn} v_{n,lm} d\Omega \quad (3.53)$$

$$\sum_e \frac{1}{2} \left\| \sqrt{\frac{J_{ijklmn}}{h}} v_{n,l} n_m^- \right\|_{L^2(\partial\Omega^e \cap \partial_I B_h)}^2 = \frac{1}{2} \int_{\partial_I B_h} \llbracket v_{k,i} \rrbracket n_j^- \frac{J_{ijklmn}}{h} \llbracket v_{n,l} \rrbracket n_m^- dS \quad (3.54)$$

where the positive semi-definite nature of  $\mathbf{C}$  and  $\mathbf{J}$  has been used.

Expression (3.51) is the norm in the constrained space because if  $\|\mathbf{v}\|$  is equal to zero, then the three contributing terms on the right hand side of the equation are also zero. The only other non trivial case for which  $\|\mathbf{v}\|$  can possibly go to zero is when  $v_h$  is piecewise linear or constant. A constant  $v_h$  will correspond to a rigid body motion, which is not allowed in the constrained space. For the case of piecewise linear  $v_h$ , the jump in derivative of displacement across the interface  $\llbracket v_{i,j} \rrbracket$  is non zero and therefore (3.51) does not vanish and hence proving (3.51) is in-fact a norm. In order to prove the stability of the method the upper bound of the bilinear  $a(\mathbf{u}, \delta\mathbf{u})$  and lower bound for the energy norm  $a(\mathbf{u}, \mathbf{u})$  need to be computed.

The upper bound of the bilinear form is established in (Appendix -B with the result

$$|a(\mathbf{u}, \mathbf{w})|^2 \leq C^k(\beta) \|\mathbf{u}\|^2 \|\mathbf{w}\|^2 \quad (3.55)$$

In this expression  $C^k$  is a constant dependent only on the degree of polynomial interpolation  $k$ . The lower bound of the bilinear form is obtained from the relation

$$\begin{aligned}
a(\mathbf{u}, \mathbf{u}) &= \sum_e \left\| \sqrt{C_{ijkl}} u_{k,l} \right\|_{L^2(\Omega^e)}^2 + \sum_e \left\| \sqrt{J_{jikqrp}} u_{p,qr} \right\|_{L^2(\Omega^e)}^2 \\
&+ \frac{\beta}{2} \sum_e \left\| \sqrt{\frac{J_{jikqrp}}{h}} \llbracket u_{p,q} \rrbracket n_r^- \right\|_{L^2(\partial\Omega^e \cap \partial_I B_h)}^2 + \left| \int_{\partial_I B_{0h}} \llbracket u_{k,i} \rrbracket \langle \tau_{jik} \rangle n_j dS \right|
\end{aligned} \tag{3.56}$$

In Appendix (B.7), we show that

$$\begin{aligned}
a(\mathbf{u}, \mathbf{u}) &\geq \sum_e \left\| \sqrt{C_{ijkl}} u_{k,l} \right\|_{L^2(\Omega^e)}^2 + \sum_e \left\| \sqrt{J_{jikqrp}} u_{p,qr} \right\|_{L^2(\Omega^e)}^2 \\
&+ \frac{\beta}{2} \sum_e \left\| \sqrt{\frac{J_{jikqrp}}{h}} \llbracket u_{p,q} \rrbracket n_r^- \right\|_{L^2(\partial\Omega^e \cap \partial_I B_h)}^2 \\
&- C^k \sum_e \left\| \sqrt{J_{jikqrp}} u_{p,qr} \right\|_{L^2(\Omega^e)} \left\| h_s^{-\frac{1}{2}} \llbracket u_{p,q} \rrbracket \sqrt{J_{jikqrp}} n_r^- \right\|_{L^2(\partial\Omega^e \cap \partial_I B_h)}
\end{aligned} \tag{3.57}$$

It follows using the  $\epsilon$ -inequality<sup>4</sup>, that the right hand side of equation (3.57) is bounded below by the expression

$$\begin{aligned}
&\sum_e \left\| \sqrt{C_{ijkl}} u_{k,l} \right\|_{L^2(\Omega^e)}^2 + (1 - \epsilon) \sum_e \left\| \sqrt{J_{jikqrp}} u_{p,qr} \right\|_{L^2(\Omega^e)}^2 \\
&+ \left( \frac{\beta}{2} - \frac{C^{k^2}}{2\epsilon} \right) \sum_e \left\| \sqrt{\frac{J_{jikqrp}}{h}} \llbracket u_{p,q} \rrbracket n_r^- \right\|_{L^2(\partial\Omega^e \cap \partial_I B_h)}^2
\end{aligned} \tag{3.58}$$

Let  $C_2(\beta) = \min \left( 1 - \epsilon, \beta - \left( C^{k^2} / \epsilon \right) \right)$ . This will become positive if  $\beta \geq C^{k^2} / \epsilon$  and

---

<sup>4</sup> $\forall \epsilon > 0 : |ab| \leq \frac{\epsilon}{2} a^2 + \frac{1}{2\epsilon} b^2$  or  $\forall \epsilon > 0 : |ab| \leq \epsilon a^2 + \frac{1}{4\epsilon} b^2$



$\epsilon < 1$ . Therefore,  $C_2(\beta) > 0$  and the bilinear form satisfies

$$a(\mathbf{u}, \mathbf{u}) \geq C_2(\beta) \|\mathbf{u}\|^2 > 0 \quad \forall u \in U_{hc}^f(B_0) \quad (3.59)$$

The above relation basically guarantees that the Null set in the solution space is the empty set.

### 3.3.3 Convergence Rate

If  $u \in U_c^f$  be the exact solution of the problem , we define  $u^k$  the interpolation of  $u$  in  $U_{hc}^f$  by

$$\int_{B_h} (\mathbf{u} - \mathbf{u}^k) \cdot \delta \mathbf{u} dV = 0 \quad \forall \delta \mathbf{u} \in U_{hc}^f \quad (3.60)$$

The error is then defined as  $\mathbf{e} = \mathbf{u}_h - \mathbf{u} \in U_c^f$ . It is assumed here that the imposed boundary condition on the dirichlet boundary is zero and strictly enforced. The Error corresponding to the interpolated solution  $\mathbf{e}^k$  is then  $\mathbf{e}^k = \mathbf{u}_h - \mathbf{u}^k \in U_{hc}^f \subset U_c^f$ . The bilinear form (B.1) are by definition linear and by using the results obtained from the upper and lower bounds of the bilinear (3.55,3.59) we obtain-

$$\begin{aligned} C_2 \|\mathbf{e}^k\|^2 &\leq a(\mathbf{u}_h - \mathbf{u}^k, \mathbf{u}_h - \mathbf{u}^k) = a(\mathbf{u}_h - \mathbf{u} + \mathbf{u} - \mathbf{u}^k, \mathbf{u}_h - \mathbf{u}^k) \\ &\leq a(\mathbf{u}_h - \mathbf{u}, \mathbf{u}_h - \mathbf{u}^k) + a(\mathbf{u} - \mathbf{u}^k, \mathbf{u}_h - \mathbf{u}^k) \\ &\leq C_1 \|\mathbf{u} - \mathbf{u}^k\| \|\mathbf{u}_h - \mathbf{u}^k\| = C_1 \|\mathbf{u} - \mathbf{u}^k\| \|\mathbf{e}^k\|, \end{aligned} \quad (3.61)$$

Here we have used equation (3.50) to show that  $a(\mathbf{u}_h - \mathbf{u}, \mathbf{u}_h - \mathbf{u}^k) = 0$ . The error bounds of  $\|\|\mathbf{u} - \mathbf{u}^k\|\|$  have been derived in Appendix (C) equation(C.5). Thus, it can be shown that the norm of the error in the energy norm is given by

$$\|\|e\|\| = \sum_e Ch_e^{k-1} |\mathbf{u}|_{\mathbf{H}^{k+1}(\partial\Omega^e)} \quad (3.62)$$

This expression demonstrates that the order of convergence is one order smaller than the polynomial approximation of the displacement field  $u$ .

### 3.4 Finite Element Implementation

In this section, the final form of the discontinuous Galerkin formulation obtained in equation (3.40) is taken as the starting point for the finite element implementation. The discontinuous Galerkin framework for strain gradient laws can be implemented within the framework of a conventional finite element solution scheme. For definiteness and ease of mesh generation, we adopt a standard 10-node quadratic tetrahedral element with second order polynomial interpolation ( $k = 2$ ). In a linear finite element solution procedure, a stiffness matrix  $K_{iakb}$  is assembled by taking into account the contributions from all the volume elements and this is used to solve a linear set of equations

$$K_{iakb}U_{kb} = f_{ia}. \quad (3.63)$$

Here  $U_{kb}$  is the nodal displacements and  $f_{ia}$  is the applied external forces on the system. In the discontinuous Galerkin formulation for strain gradient elasticity, apart

from the regular finite elements over the volume of the domain, it is required to compute the integrals over interelement surfaces ( $\partial\Omega_e \cap \partial_I B_0$ ) and part of the boundary where higher order Dirichlet condition is imposed ( $\partial\Omega_e \cap \partial_M B_0$ ). In our implementation, assembly process to obtain the global stiffness matrix is from the volume elements  $K_{iakh}^e$  is followed by the assembly of contributions from the internal interface element and the assembly of contributions from the external boundary interface elements.

The conventional assembly process to obtain the global stiffness matrix is now performed over the volume elements then over all the internal interface element  $K_{iakh}^I$  and finally over all the boundary interface elements  $K_{iakh}^B$ .

$$K_{iakh} = \sum_e K_{iakh}^e + \sum_I K_{iakh}^I + \sum_B K_{iakh}^B \quad (3.64)$$

Note that the summations here imply an assembly of local stiffness matrices into the global stiffness matrix.

The contributions to the stiffness matrix from the volume elements comprises the conventional low-order virtual work of the low-order stress doing work on the low order strain. But for the strain gradient formulation, the virtual work of the high-order stress acting on the high-order strain must be considered  $\int_{\Omega_e} w_{k,ij} \tau_{jik} d\Omega$ . The implementation of the high-order term requires the computation of the second derivatives of the shape functions inside the element. The derivation of the second derivatives of the shape functions  $N_{a,ij}$  for an iso-parametric tetrahedral element is provided in Appendix D. The second derivatives of the interpolated displacement and

the displacement and the test function field can then be written as

$$u_{i,jk} = \sum_{a=1}^{10} N_{a,jk} U_{ai} \quad (3.65)$$

$$w_{i,jk} = \sum_{a=1}^{10} N_{a,jk} W_{ai}, \quad (3.66)$$

where  $U_{ai}, W_{ai}$  correspond to the nodal values of displacements and test function respectively. With this the higher order volume element's stiffness term can be expressed as  $\int_{\Omega_e} N_{a,ij} J_{jikmnl} N_{b,mn} d\Omega$ . The contribution to the global stiffness matrix from each volume element then follows as

$$K_{akbl}^V = \int_{\Omega_e} (N_{a,ij} J_{jikmnl} N_{b,mn} + N_{a,i} C_{iklm} N_{b,m}) d\Omega. \quad (3.67)$$

The contribution to the global stiffness matrix from the surface terms in equation (3.40) is most suitably implemented by recourse to the so-called *interface elements*. The main advantage of performing the surface integral using an interface element is that they can be naturally added to any finite element code as a different type of element without major modifications to the element stiffness matrix computation, assembly and solver. Interface elements have been previously employed in a  $C^0$  discontinuous Galerkin formulation for solids [25].

In this case, the formulation allows for discontinuities in the displacement field itself. This requires splitting up of the mesh in a way that each element has its own nodes which are not shared with any other volume element. Among the implications of that formulation is an explosion of the number of degrees of freedom in the

computational mesh and thus, in the over all computational cost.

However in the formulation for nonlocal elasticity presented in this work. the discontinuous Galerkin method's concept is exploited for the purpose of enforcing the interelement  $C^1$  continuity requirement in a weak manner, whereas  $C^0$  continuity is enforced strongly, i.e. , the displacement field is assumed continuous at the interelement boundaries. Consequently, the mesh nodes are shared between adjacent volume element. An interface element is shown in the figure (3.2). At each and every internal inter-element boundary an interface element is inserted. In addition to the nodes present on the interelement boundary, these interface elements require information about the adjacent tetrahedra and suitable data structures to hold it. The necessary information arises from a consideration of the quantities involved in the surface integral terms in equation (3.40). Specifically,  $[[u_{i,j}]]$ ,  $\langle \tau_{ijk} \rangle$ ,  $[[w_{i,j}]]$  and  $n_i$  on the interface element. The jump in the derivative of the displacement at an interface element is the difference in derivative of the displacement computed by the two tetrahedra which lie adjacent to a interface element.

$$[[u_{i,j}]] = \sum_{a^+} N_{a,j}^+ U_{ia} - \sum_{a^-} N_{a,j}^- U_{ia} \quad (3.68)$$

and similarly for the derivatives of displacements, the derivatives of test functions

$$[[w_{i,j}]] = \sum_{a^+} N_{a,j}^+ W_{ia} - \sum_{a^-} N_{a,j}^- W_{ia} \quad (3.69)$$

Following similar arguments, the mean high-order stresses can be expressed as

$$\langle \tau_{ijk} \rangle = \frac{1}{2} \left( \sum_{a^+} J_{ijkqrp}^+ N_{a,qr}^+ U_{ap} + \sum_{a^1} J_{ijkqrp}^- N_{a,qr}^- U_{ap} \right). \quad (3.70)$$

Observing equations (3.68-3.70) it becomes evident that the limiting values of the first

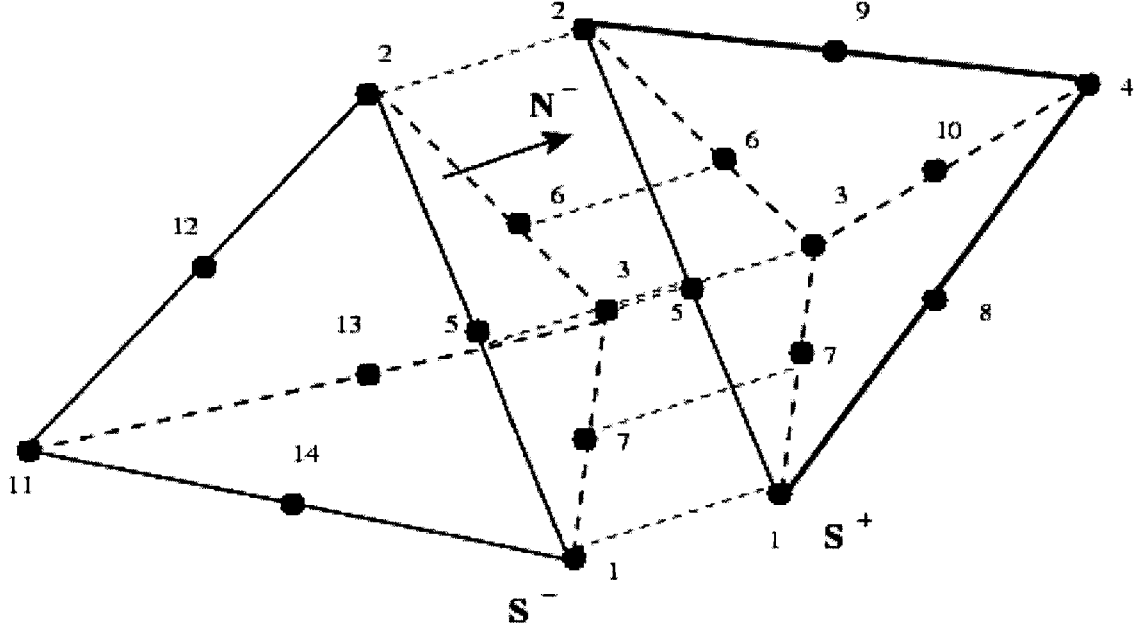


Figure 3.2: Interface Element with the two adjacent tetrahedra

and second derivatives of the shape functions and of the higher order elasticity tensor  $J_{ijkpqr}$  are required at the integration points of the interelement boundary. In our implementation, the limiting values of the shape functions at the surface quadrature points are also computed and stored during the conventional evaluation of the shape functions at the volume interpolation points. The total storage requirement for a tetrahedra is equal to the number of quadrature points in the bulk ( $N_\xi$ ) plus the number of faces ( $N_{facet}$ ) times the number of quadrature points on the surface ( $N_\zeta$ ). In our case  $N_\xi = 4$  and  $N_\zeta = 6$  and for a tetrahedra  $N_{facet} = 4$ . In order to do this,

each interface element requires the connectivity of the two adjacent tetrahedra and the nodes they share with the tetrahedron.

In our implementation we make intensive use of the *Boundary representation of solids (B-Rep)* to efficiently generate these data structures from the mesh topology. The advantage of using a *B-Rep* data structure is that no modification is required to the geometric description of the body, the *B-Rep* array takes in the *coordinate table* and *connectivity table* and creates linked list data structures of all the tetrahedra , facets and edges present in the mesh [31, 32]. At each interface the connectivity of

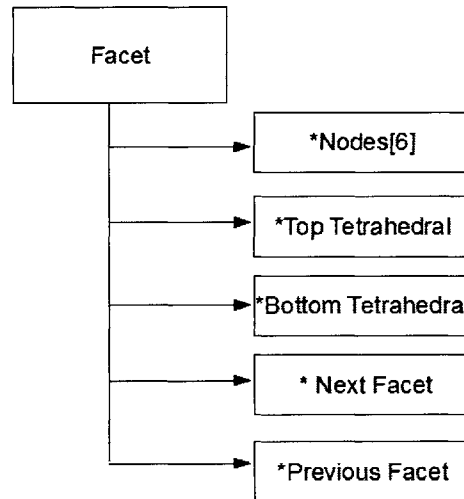


Figure 3.3: Data structure for Storing facet information

all the nodes present in the two adjacent tetrahedra is needed to access the shape functions and their derivatives on the interface element. This is made possible by knowing the relative mapping of the nodes which lie on the interface to the adjacent tetrahedra and the global ID of the adjacent tetrahedra.

The geometry of the interface element required to compute the normals and to define the domain on which the surface integrals are computed is interpolated from

the surface element using the standard surface shape functions.

This information is extracted from the *facet* data structure, figure (3.3), which is generated by the *B-Rep*. In the interface element, the interpolation of position, the evaluation of Gauss integration weights and the computation of normals are done using the the standard surface shape functions of the interface element  $N_a(\xi)$ ,  $a \in [1, n]$ , where  $\xi = (\xi_1, \xi_2)$  are the natural coordinates. The outer unit normal  $\mathbf{n}^-$  corresponding to element  $\Omega_0^{e-}$  is given by

$$\mathbf{n}^-(\xi) = \frac{\mathbf{G}_1(\xi) \times \mathbf{G}_2(\xi)}{|\mathbf{G}_1(\xi) \times \mathbf{G}_2(\xi)|} \quad (3.71)$$

in which

$$\mathbf{G}_\alpha(\xi) = \mathbf{X}_\alpha = \sum_{a=1}^n N_{a,\alpha}(\xi) \mathbf{X}_a \quad (3.72)$$

are the covariant base vectors,  $\alpha \in [1, 2]$ . The limiting values of the volume stresses, displacements and shape functions at the interelement boundaries  $\pm$  required to compute the mean stresses and gradient of displacement and gradient of test function jumps; are obtained directly from the interpolation of volume element fields evaluated on the surface element integration points.

The preceding expressions for the various quantities involved in the surface terms of the weak form:  $\int_{\partial_I \Omega} \llbracket w_{k,i} \rrbracket \left( \langle \tau_{jik} \rangle n_j + n_j \left\langle \frac{\beta J_{jikqrp}}{h} \right\rangle \llbracket u_{p,q} \rrbracket n_r \right) dS$  lead to the contribution of the interface element to the stiffness matrix given by the expressions

$$K_{akbp}^{I++} = \int_{\partial_I \Omega} N_{a,i}^+ \left( \frac{1}{2} J_{jikqrp}^+ N_{b,qr}^+ n_j + n_j \left\langle \frac{\beta J_{jikqrp}}{h} \right\rangle N_{b,q}^+ n_r \right) dS \quad (3.73)$$



$$K_{akbp}^{I+-} = \int_{\partial_I \Omega} N_{a,i}^+ \left( \frac{1}{2} J_{jikqrp}^- N_{b,qr}^- n_j - n_j \left\langle \frac{\beta J_{jikqrp}}{h} \right\rangle N_{b,q}^- n_r \right) dS \quad (3.74)$$

$$K_{akbp}^{I-+} = - \int_{\partial_I \Omega} N_{a,i}^- \left( \frac{1}{2} J_{jikqrp}^+ N_{b,qr}^+ n_j + n_j \left\langle \frac{\beta J_{jikqrp}}{h} \right\rangle N_{b,q}^+ n_r \right) dS \quad (3.75)$$

$$K_{akbp}^{I--} = - \int_{\partial_I \Omega} N_{a,i}^- \left( \frac{1}{2} J_{jikqrp}^- N_{b,qr}^- n_j - n_j \left\langle \frac{\beta J_{jikqrp}}{h} \right\rangle N_{b,q}^- n_r \right) dS \quad (3.76)$$

where  $+(-)$  represents the nodes on the top (bottom) tetrahedron. Directing attention towards the application of boundary conditions in the discontinuous Galerkin formulation, the essential boundary condition on the displacement  $\bar{u}_k$  is enforced strongly on  $\partial_D B_0$  by simply eliminating appropriate nodal degrees of freedom and imposing the value of the displacement, just as in a conventional finite element program. The low order traction boundary condition  $\hat{t}_k$  contributes to the external applied force array  $f_{ak}$  on  $\partial_N B_0$ :

$$f_{ak}^e = \int_{\partial \Omega_e \cap \partial_N B_0} N_a \hat{t}_k dS \quad (3.77)$$

also in a conventional fashion. The double stress traction  $\hat{r}_k$  on  $\partial_M B_0$  contributes to the externally applied force array  $f_{ak}$

$$f_{ak}^e = \int_{\partial \Omega_e \cap \partial_M B_0} N_{a,l} n_l \hat{r}_k dS \quad (3.78)$$

It should be noted that in contrast to the low order traction boundary condition

which involves the values of the shape functions, the gradients of shape functions appear in the expression for the case of higher order boundary conditions. As a result all the volume element nodes adjacent to the boundary  $\partial_M B_0$  and not just the subset lying on the surface carry contributions of the externally applied force array. From the final form of the weak form obtained in equation (3.40), the normal component of the displacement gradient  $\overline{Du}_k$  specified on the external surface  $\partial_T B_0$  will contribute terms both to the stiffness matrix  $K_{iakb}^b$  and to the external force array  $f_{ia}^e$ . The elemental stiffness matrix for a specified normal component of the displacement gradient is given by

$$K_{akbp}^b = - \int_{\partial\Omega_e \cap \partial_T B_0} N_{a,l} n_l n_i \left[ n_j J_{jikqrp} N_{b,qr} + n_j \frac{\beta J_{jikqrp}}{h} n_s N_{b,s} n_q n_r \right] dS \quad (3.79)$$

whereas the corresponding contributions to the external force array is given by

$$f_{ak}^e = - \int_{\partial\Omega_e \cap \partial_T B_0} N_{a,l} n_l n_i n_j \frac{\beta J_{jikqrp}}{h} \overline{Du}_p n_q n_r dS \quad (3.80)$$

The preceding expressions of various contributions to the force arrays and stiffness matrix from the surface terms was implemented as part of the assembly process of the interface elements in our research finite code.

This concludes the discussion of the finite element implementation of the discontinuous Galerkin formulation for strain gradient elasticity. In the next chapter, numerical convergence tests and verification examples are presented.

# Chapter 4

## Numerical tests and examples

In this section, a number of numerical tests are conducted for the purpose of verifying the numerical properties of the discontinuous Galerkin formulation and for demonstrating size effect in strain gradient constitutive laws. To this end, the exact analytical solution of two simple unidimensional problems in nonlocal elasticity are derived and used for comparison with the numerical simulation. A simple linear constitutive law relating both high and low order stresses and strains of the form

$$\sigma_{ij} = C_{ijkl} \epsilon_{kl} \quad (4.1)$$

$$\tau_{ijk} = J_{ijklmn} \eta_{lmn} \quad (4.2)$$

are employed. The length scale parameter  $l$  is engulfed in the higher order stiffness matrix  $J_{ijklmn}$ . The expression for  $J_{ijklmn}$  is explicitly written in appendix A. The closed form solution of the unidimensional problems used as a basis for verification of the numerical methods are derived in Appendix E. Although the example problems

are unidimensional the numerical tests are conducted with the full three-dimensional implementation in our research finite element code.

## 4.1 Tension Test

In this example, a prismatic bar with a rectangular cross-section as shown in figure (4.1) is subjected to simple tension by applying constraints at the left end and displacement boundary condition at the right end. The geometric dimensions and the material model properties are given in table (4.1). In addition to the standard low order boundary conditions, higher order boundary conditions are necessary at all points on the boundary. Just as is the case with the homogeneous low order natural boundary condition the high order homogeneous natural boundary condition is automatically specified.

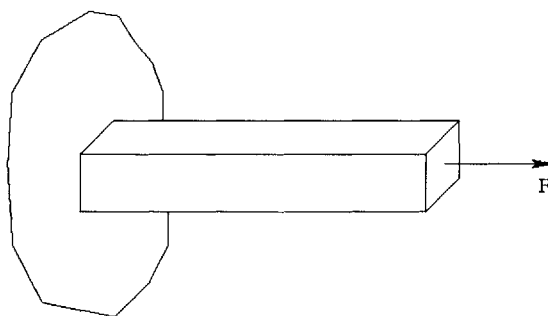


Figure 4.1: Tensile test problem

$$r_k = 0 \tag{4.3}$$

This example constitutes a patch test consisting of a constant stress state, and thus, does not exhibit any gradient (size) effects. The analytical solution for the problem is

derived in Appendix (E). Figure (4.2) shows a comparison of the length-wise distri-

Properties	values
Length	$L = 1m$
Height	$h = 0.1m$
Young modulus	$E = 70GPa$
Poisson ratio	$\nu = 0.3$
Nonlocal constants	$a_1 = a_2 = a_3 = a_4 = 1$
Length scale parameter	$l = 0.1m$
Stabilization parameter	$\beta = 10$

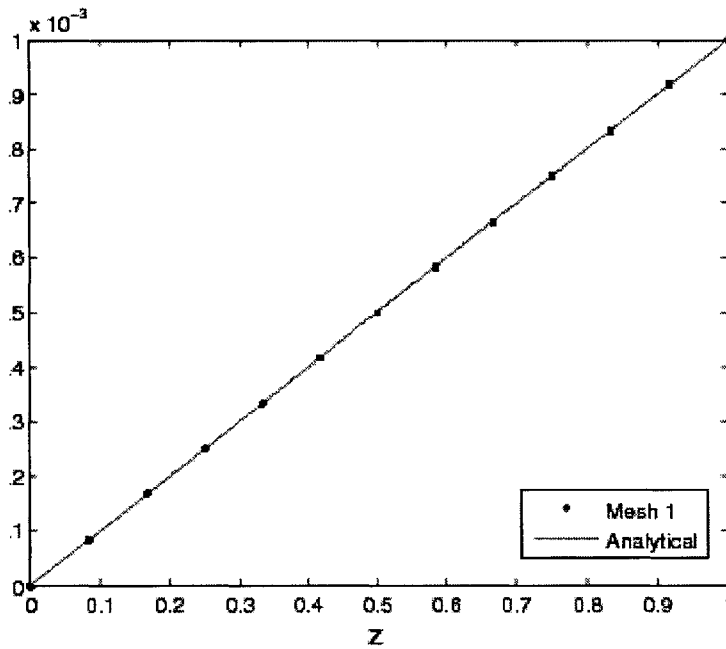


Figure 4.2: comparison of  $u_z$  along  $z$  axis of mesh 1 in 4.4 subjected to an tensile load and the analytical solution for the unidimensional tensile load problem

bution of the displacement field  $u_z$ . It can be observed in this figure that the numerical solution matches exactly the analytical solution, as required for convergence.

## 4.2 Bi-material tensile test

The numerical properties of the discontinuous Galerkin formulation are studied in the presence of gradient effects. To this end, we consider a prismatic beam made up of two materials as illustrated in figure (4.3) with a uniform square cross-section subjected to a tensile load. The geometric dimensions and material properties are listed in table (4.2). The analytical solution for this problem is derived in Appendix (E) where the nonlocal features of the solution are also discussed. The simulations are run for

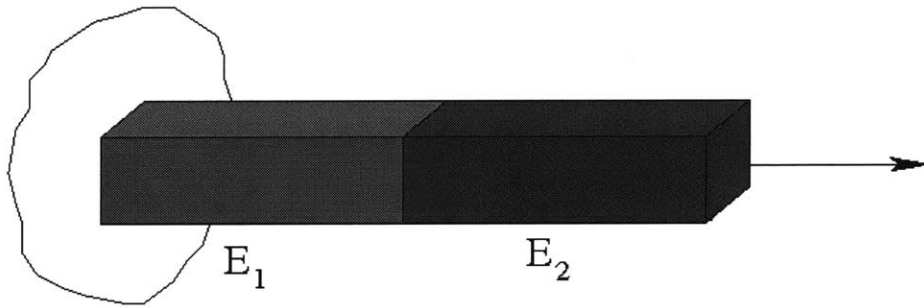


Figure 4.3: Bi-material tensile loading test

different mesh sizes as illustrated in Figure 4.4. The displacement field  $u_z$  along the  $z$  axis is compared with the analytical solution for different mesh sizes in Figure 4.5. It can be observed that even for a very coarse mesh the error in displacement is very small. The normal strain component along the  $z$  axis  $\epsilon_{zz}$  is plotted for various mesh sizes and compared with the analytical solution in figure (4.6). In order to assess the convergence properties in a quantitative manner, the  $L^2$  norm of error in the displacement is computed using the nodal displacement values obtained from the finite element solution and the analytical solution. The plot of is presented in figure (4.7). It is seen that the rate of convergence is two. The resulting strain field

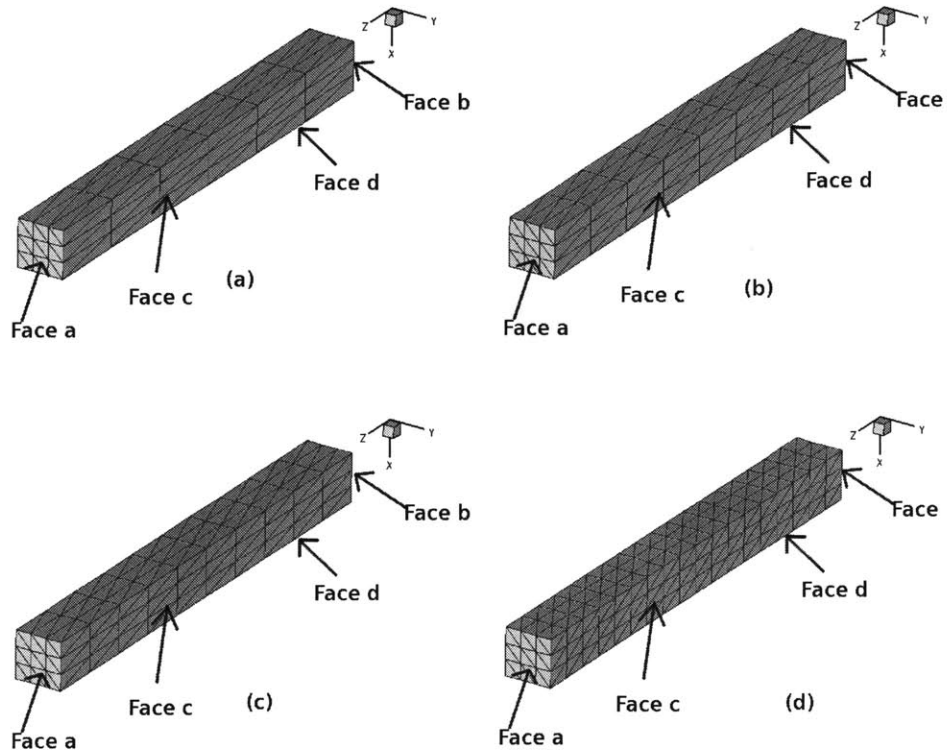


Figure 4.4: Tensile test problem discretization employed (a) mesh 1 ;(b) mesh 2; (c) mesh 3; (d) mesh 4.

Properties	values
Length	$L = 1m$
Height	$h = 0.1m$
Young modulus	$E_1 = 70GPa, E_2 = 280GPa$
Poisson ratio	$\nu_1 = 0.3, \nu_2 = 0.3$
Nonlocal constants	$a_1 = a_2 = a_3 = a_4 = 1$
Length scale parameter	$l = 0.1m$
Stabilization parameter	$\beta = 10$

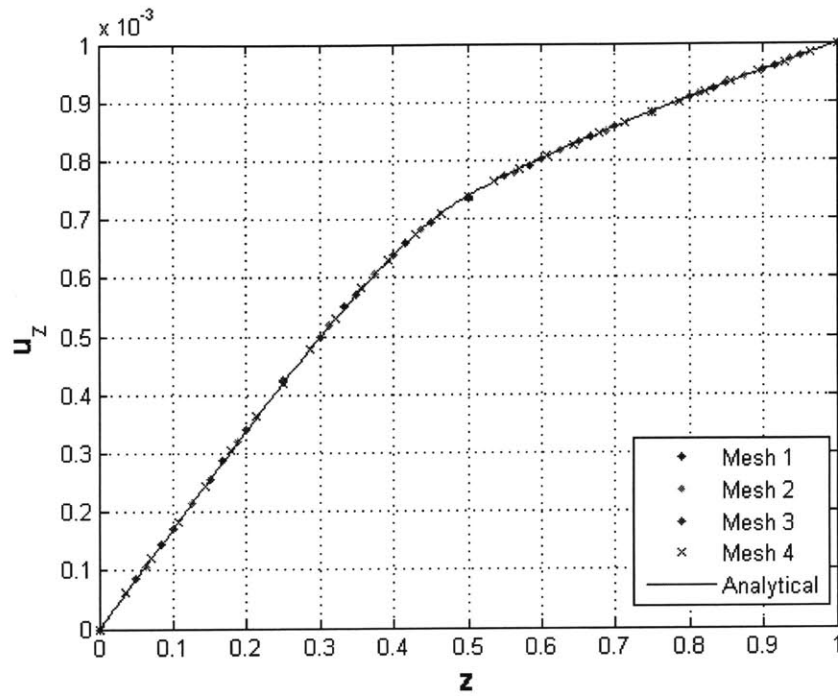


Figure 4.5: Displacement profile for a bi material specimen subjected to tensile load

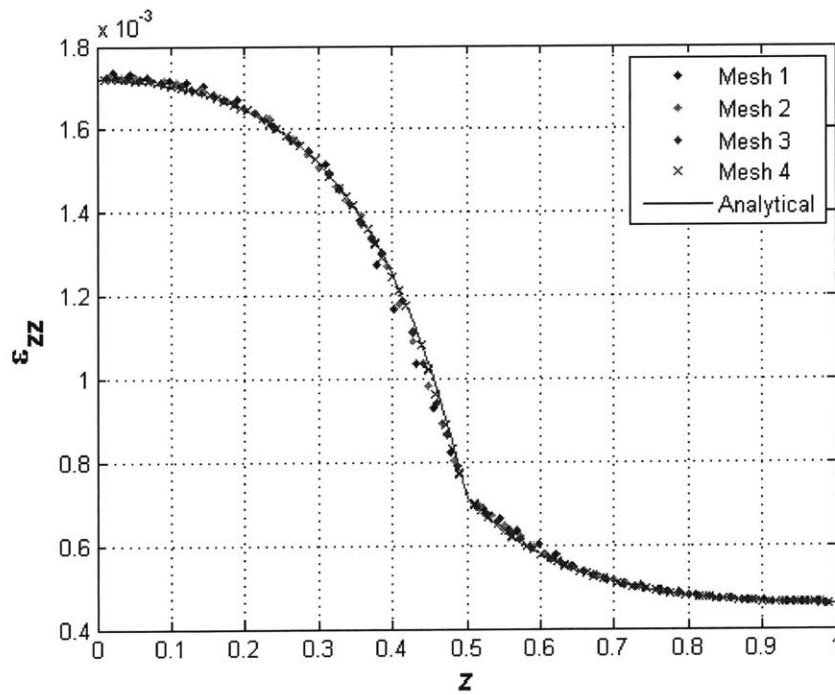


Figure 4.6: Strain profile for a bi material specimen subjected to tensile load



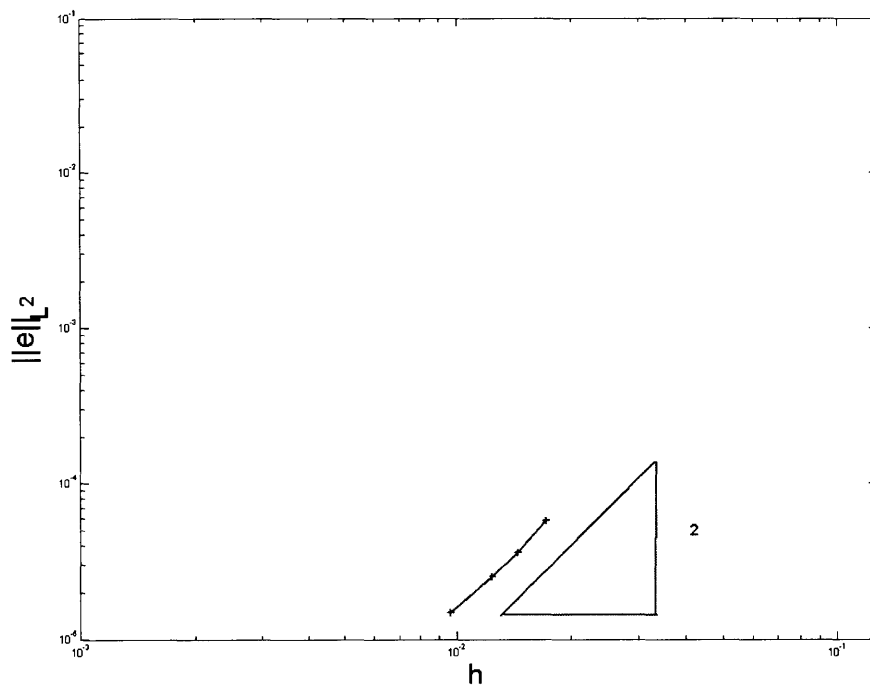


Figure 4.7: Convergence analysis:  $L^2$  norm of the displacement error v/s mesh size

exhibits size effects i.e. a dependence on the size of the specimen subjected to a simple tensile load. The presence of the gradient terms smooths the strain field in the problem domain in comparison to the local linear elastic constitutive laws. The effect of the size parameter on the strain profile is studied by running simulations varying the length scale parameter  $l$  with all other geometric and material properties remaining the same. For this purpose, the fine mesh shown in figure (4.4-d) is employed. The

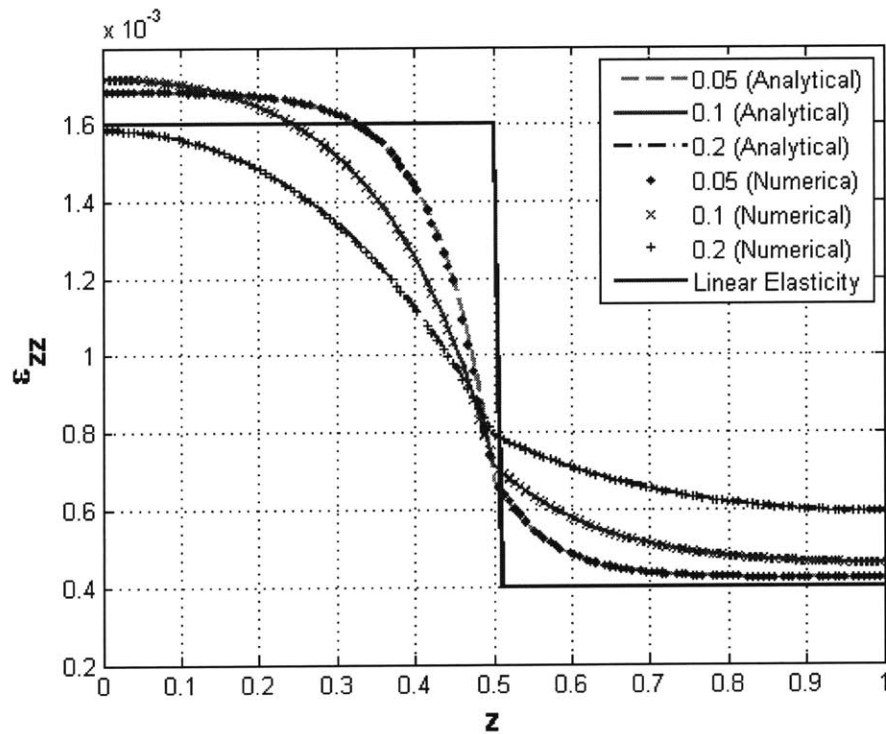


Figure 4.8: Comparison of numerical and analytical results of strain profile along the  $z$  axis for three different values of  $\frac{l}{L}$ .

effect of varying  $\frac{l}{L}$  is shown in figure (4.8). As the ratio of  $\frac{l}{L}$  is decreased the strain profile approaches the case of linear elasticity and when this ratio is increased the difference between the maximum and minimum strains in the domain is decreases until it becomes a constant in the domain.

### 4.3 Clamped Beam under bending loading

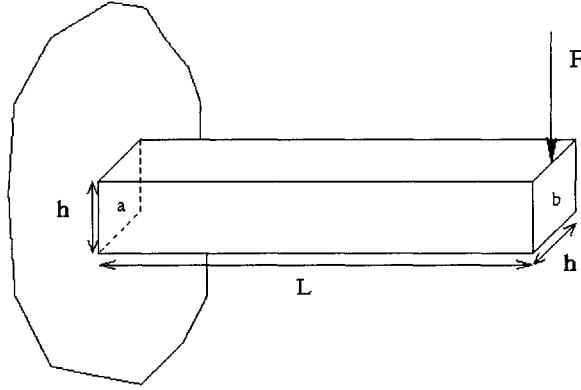


Figure 4.9: Bending problem illustration

In this section the effect of length scale parameter on the bending stiffness of a cantilever beam is demonstrated. The presence of gradient terms in the constitutive relation helps to smooth the strain field and thus affects the bending stiffness [14]. To this end, we consider an uniform prismatic beam with a rectangular cross-section which is entirely clamped at one end and subjected to a bending force at the other end. The higher order conditions are the tractions set to zero, equation (4.3). The geometry and the material properties of the beam are listed in table (4.3). In classical

Table 4.3: Bending test material properties

Properties	values
Length	$L = 1m$
Height	$h = 0.1m$
Young modulus	$E = 70GPa$
Poisson ratio	$\nu = 0.3$
Nonlocal constants	$a_1 = a_2 = a_3 = a_4 = 1$
Stabilization parameter	$\beta = 10$

linear elasticity for thin beams the tip deflection ( $\delta$ ) corresponding to an applied load

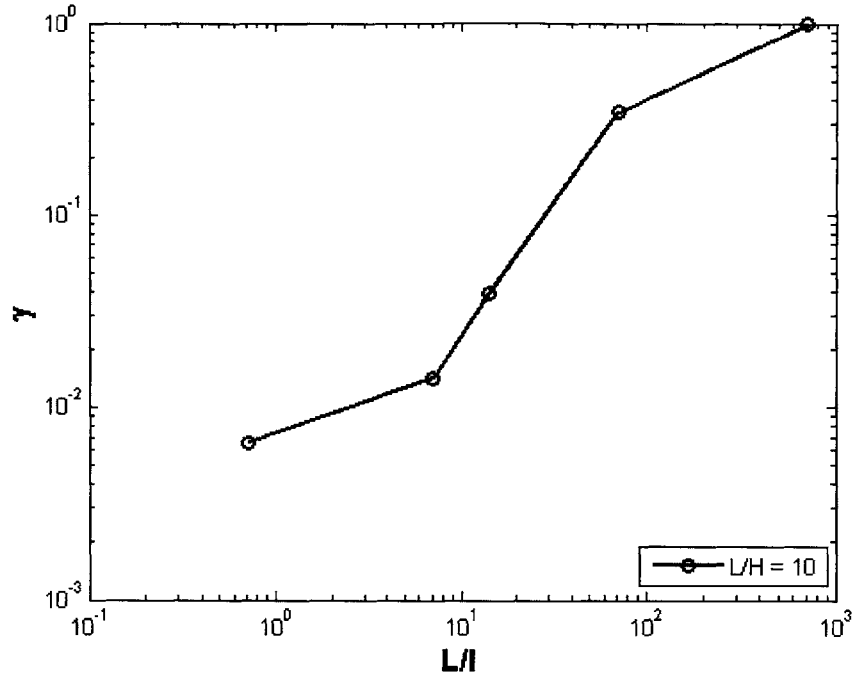


Figure 4.10: Plot of stiffness ratio to the ratio of length of the beam to the length scale parameter

( $F$ ) is given by

$$\delta = F \frac{L^3}{3EI} \quad (4.4)$$

where  $E$  is the elastic moduli of the beam,  $I$  is the moment of inertia of the cross-section,  $L$  is the length of the beam. Rearranging equation (4.4) the bending stiffness can be expressed as

$$K_e = \frac{F}{\delta} = \frac{3EI}{L^3} \quad (4.5)$$

here  $K_e$  refers to the linear elastic thin beam bending stiffness. The effect of the gradient term can be studied by plotting the ratio of stiffness in the linear elastic case ( $K_e$ ) to the stiffness exhibited by the beam with the gradient terms ( $F/\delta$ ), and

this ratio is defined as the stiffness ratio and indicated with the symbol  $\gamma$ .

$$\gamma = \frac{K_e \delta}{F} \tag{4.6}$$

Stiffness ration  $\gamma$  is plotted with respect to the ratio of  $(l/L)$ ,  $l$  being the size factor and  $L$  being the length of the beam (4.10). All the *dof's* are restrained along *face a* in figure (4.9) and a force is applied to all nodes on *face b*. As the the length scale parameter  $l$  increases and becomes comparable to the length of the beam  $L$ , the bending stiffness of the beam increases.

## 4.4 Size effects under torsion

In this section, the size effect of the strain gradient law is once again demonstrated with a torsion example. A prismatic bar of uniform square cross-section is subjected to a pure torsional load, which are specified using the appropriate boundary conditions figure (4.11). The geometric and material properties of the beam is given in table (4.4). To study the effect of size effect on the shear moduli of the nonlocal linear elastic

Table 4.4: Torsion test geometric and material properties

Properties	values
Length	$L = 1m$
Height	$h = 0.1m$
Young modulus	$E = 70GPa$
Poisson ratio	$\nu = 0.3$
Nonlocal constants	$a_1 = a_2 = a_3 = a_4 = 1$
Angle of twist	$\theta = 1^\circ$
Stabilization parameter	$\beta = 10$

material we plot the ratio of the shear moduli as obtained in the linear elastic case

to the strain gradient elastic case ( $\gamma$ ). In order to carry out the numerical simulation a uniform tetrahedral mesh as illustrated in figure (4.12). The torsion problem is simulated for the material length scale parameter varying from  $10^{-4} - 10^{-1}$ . This variation in  $\gamma$  is plotted against the ratio of width of the beam to the length scale parameter: figure (4.13). Observing figure (4.13) its seen that the, shear moduli of

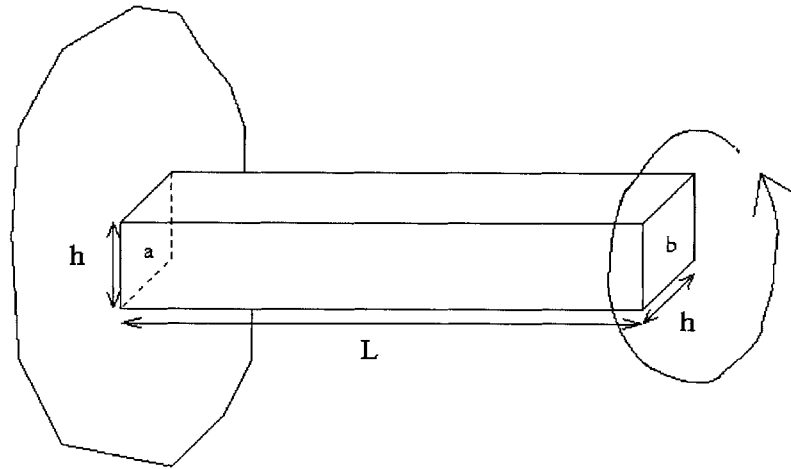


Figure 4.11: Description of the problem setup for torsional loading of a prismatic beam of square cross-section

the beam increases as the size parameter is increased when keeping all other geometric and material parameters constant.

This concludes the discussion on the Numerical results, in the next chapter conclusions and future work is presented.

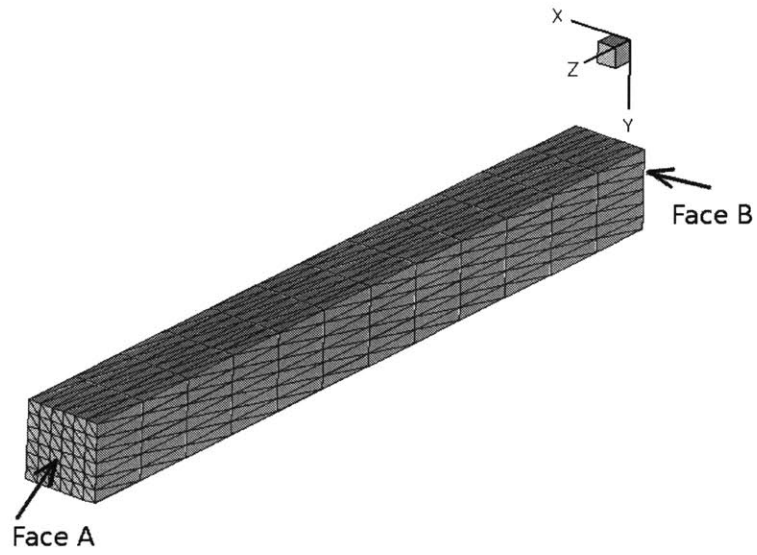


Figure 4.12: An illustration of the mesh used in the torsion example

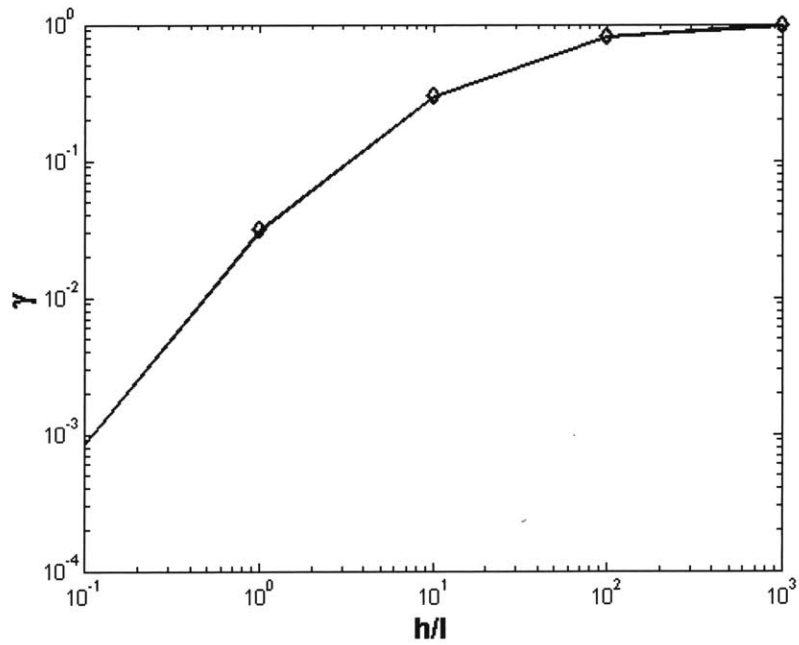


Figure 4.13: Plot of torsion stiffness ratio  $\gamma$  to the ratio of thickness of the beam to the length scale parameter





# Chapter 5

## Conclusions

In this work an implementation of low order discontinuous Galerkin method for non linear hyperelasticity was developed in three dimensions and convergence properties where studied with suitable examples.

A discontinuous Galerkin formulation for nonlocal linear strain gradient law was formulated and implemented in three dimensions. The stability and convergence of the discontinuous Galerkin formulation were derived analytically and demonstrated with suitable numerical examples. The size effect exhibited by strain gradient laws where demonstrated with the help of suitable numerical examples. It is found that the formulation proposed provides a versatile approach for the discretization of the higher order theories and will provide a better platform to handle non-linearities which will arise in the case of plasticity and problems involving crack propagation.

In extending this work firstly on the implementation side, the present implementation can only handle a very trivial higher order boundary condition corresponding to the case of double stress traction being zero at all points on the boundary. Routines

to handle the higher order essential and natural conditions have to be implemented. On the formulation side, the next logical extension of the work would be to adapt the discontinuous Galerkin formulation for small deformation strain gradient plasticity and then explore the extension to finite strain gradient elasticity and plasticity.

Possibilities exist in extending the formulation for explicit problems and study the effect of the DG formulation on critical time step and stability of time stepping algorithms. It is still not clear as to how the effect of nonlocal terms will affect the parallelization of the finite element codes and more work is needed in the direction for explicit problems. On the analytical side of the problem, more efforts are needed to compute posteriori error estimates for problems with strain gradient laws. On the geometric side, most of the mesh node numbering optimization codes to minimize bandwidth of the stiffness matrix take into account only the volume elements, it will be interesting to develop mesh node numbering optimization codes that take into account the interface elements as well.

# Bibliography

- [1] D.N. Arnold, F. Brezzi, B. Cockburn, and L.D. Marini. Unified analysis of discontinuous Galerkin methods for elliptic problems. *SIAM Journal of Numerical Analysis*, 39(5):1749–1779, 2002. missing, DOI.
  
- [2] D.N. Arnold, F. Brezzi, and L. D. Marini. A family of discontinuous Galerkin finite elements for the Reissner-Mindlin plate. *Journal of Scientific Computing*, 22-23:25–45, 2005. pdf, DOI.
  
- [3] F. Bassi and S. Rebay. A high-order accurate discontinuous finite element method for the numerical solution of the compressible Navier-Stokes equations. *Journal of Computational Physics*, 131:267–279, 1997. pdf, DOI.
  
- [4] S.C. Brenner and L.-Y Sung. C0 interior penalty methods for fourth order elliptic boundary value problems on polygonal domains. *J. Sci. Comput.*, 22-23(1-3):83–118, 2005. pdf, DOI.
  
- [5] F. Brezzi, B. Cockburn, L.D. Marini, and E. Tamma, Süli. Stabilization mechanisms in discontinuous Galerkin finite element methods. *Computer Methods in Applied Mechanics and Engineering*, 195:3293–3310, 2006. pdf, DOI.

- [6] F. Brezzi, G. Manzini, D. Marini, P. Pietra, and A. Russo. Discontinuous Galerkin approximations for elliptic problems. *Numerical Methods for Partial Differential Equations*, 16(4):365–378, 2000. pdf, no DOI.
- [7] F. Celiker and B. Cockburn. Element-by-element post-processing of discontinuous galerkin methods for timoshenko beams. *Journal of Scientific Computing*, 27(1–3):177–187, 2007. pdf, DOI.
- [8] G Engel, K. Garikipati, T.J.R. Hughes, M.G. Larson, L Mazzei, and RL Taylor. Continuous/discontinuous finite element approximations of fourth-order elliptic problems in structural and continuum mechanics with applications to thin beams and plates. *Computer Methods in Applied Mechanics and Engineering*, 191:3669–3750, 2002. pdf, DOI.
- [9] F. Brezzi, M. Fortin. *Mixed and Hybrid Finite Element Methods*. Springer, Berlin, 1991.
- [10] N.A. Fleck and J.W. Hutchinson. Strain gradient plasticity. *Advances in Applied Mechanics*, 33:295–361, 1997. pdf, DOI.
- [11] S. Güzey, B. Cockburn, and H.K. Stolarski. The embedded discontinuous Galerkin method: Application to linear shell problems. *International Journal for Numerical Methods in Engineering*, 2007. pdf, DOI.
- [12] S. Güzey, H.K. Stolarski, B. Cockburn, and K.K. Tamma. Design and development of a discontinuous Galerkin method for shells. *Computer Methods in Applied Mechanics and Engineering*, 195:3528–3548, 2006. pdf, DOI.

- [13] P Hansbo and MG Larson. Discontinuous Galerkin methods for incompressible and nearly incompressible elasticity by Nitsche’s method. *Computer Methods in Applied Mechanics and Engineering*, 191:1895–1908, 2002. pdf, DOI.
- [14] Harm Askes and Elias C. Aifantis. Numerical modeling of size effects with gradient elasticity- Formulation, meshless discretization and examples. *International Journal of Fracture*, 117:347–358, 2002. pdf, doi.
- [15] J. Y. Shu and N. A. Fleck. Prediction of a size effect in micro indentation. *International Journal of Solids and Structures*, 35:1363–1383, 1998. pdf, doi.
- [16] John. Y. Shu, Wayne E. King and N. A. Fleck. Finite elements for materials with strain gradient effects. *International Journal for Numerical Methods in Engineering*, 44:373–391, 1999. pdf, doi.
- [17] L. Anand, M.E. Gurtin, S. P. Lele, C. Gething. A one-dimensional theory of strain-gradient plasticity: Formulation, analysis, numerical results. *Journal of Mechanics and Physics of Solids*, 53:1789–1826, Aug. 2005. pdf, doi.
- [18] A. Lew, P. Neff, D. Sulsky, and M. Ortiz. Optimal BV estimates for a discontinuous Galerkin method for linear elasticity. *Applied Mathematics Research eXpress*, 3:73–106, 2004. pdf, no DOI.
- [19] M.E. Gurtin. A gradient theory of small-deformation isotropic plasticity that accounts for the Burgers vector and for dissipation due to plastic spin. *Journal of Mechanics and Physics of Solids*, 52:2245–2568, 2004. pdf, doi.

- [20] Mindlin, R.D. Second Gradient of Strain and Surface-Tension in Linear Elasticity. *International Journal of Solids and Structures*, 1:417–438, 1965. pdf, No doi.
- [21] L. Molari, G.N. Wells, K. Garikipati, and F. Ubertini. A discontinuous Galerkin method for strain gradient-dependent damage: Study of interpolations and convergence. *Computer Methods in Applied Mechanics and Engineering*, 195:1480–1498, 2006. pdf, DOI.
- [22] N. A. Fleck and J. W. Hutchinson. A reformulation of strain gradient plasticity. *Journal of Mechanics and Physics of Solids*, 49:2245–2271, 2001. pdf, doi.
- [23] JA Nitsche. Über ein variationsprinzip zur Lösung Dirichlet-Problemen bei Verwendung von Teilräumen, die keinen Randbedingungen uneworfen sind. *Abhandlungen aus dem Mathematischen Seminar der Universität Hamburg*, 36:9–15, 1971.
- [24] L. Noels and R. Radovitzky. A new discontinuous galerkin method for kirchhoff-love shells. Part I: Formulation. *Computer Methods in Applied Mechanics and Engineering*. Submitted, no pdf, no DOI.
- [25] L. Noels and R. Radovitzky. A general discontinuous Galerkin method for finite hyperelasticity. Formulation and numerical applications. *International Journal for Numerical Methods in Engineering*, 68(1):64–97, 2006. pdf, DOI.

- [26] L. Noels and R. Radovitzky. Alternative approaches for the derivation of discontinuous galerkin methods for nonlinear mechanics. *Journal of Applied Mechanics*, 2007. accepted, pdf.
- [27] L. Noels and R. Radovitzky. An explicit discontinuous galerkin method for non-linear solid dynamics. formulation, parallel implementation and scalability properties. *International Journal for Numerical Methods in Engineering*, 2007. Submitted, no pdf, no DOI.
- [28] O. C. Zienkiewicz and R. L. Taylor . *The Finite Element method, 4th edn.* McGraw-Hill, New York, 1994.
- [29] R. A. Toupin. Elastic materials with couple stresses. *Arch. Rational Mech. Anal.*, 11:385–414, 1962.
- [30] R. D. Mindlin. Micro-structure in linear elasticity. *Arch. Rational Mech. Anal.*, 16:51–78, 1964.
- [31] R. Radovitzky, M. Ortiz. Tetrahedral mesh generation based on node insertion in crystal lattice arrangements and advancing-front-Delaunay triangulation. *Computer Methods in Applied Mechanics and Engineering*, 187:543–569, 2000. pdf, doi.
- [32] R. Radovitzky and M. Ortiz. Error estimation and adaptive meshing in strongly nonlinear dynamic problems. *Computer Methods in Applied Mechanics and Engineering*, 172:203–240, 1999. pdf, DOI.

- [33] WH Reed and TR Hill. Triangular mesh methods for the neutron transport equation. Technical Report LA-UR-73-479, Los Alamos Scientific Laboratory, 1973.
- [34] S.C.Brenner, L. Sung. Linear finite element methods for planar linear elasticity. *Math. Comp.*, 59:321–338, 1992. pdf.
- [35] Tang, Z. and Shen, S. and Atluri, S.N. Analysis of Materials with Strain-Gradient Effects: A Meshless Local Petrov-Galerkin (MLPG) Approach, with nodal displacements only. *Computer Methods in Engineering and Sciences* , 4:177–196, 2003. pdf, DOI.
- [36] A. Ten Eyck and A. Lew. Discontinuous Galerkin methods for non-linear elasticity. *International Journal for Numerical Methods in Engineering*, 67:1204–1243, 2006. pdf, DOI.
- [37] Ulrik Borg and Norman A Fleck. Strain gradient effects in surface roughening. *Modelling and Simulation in Materials Science and Engineering*, 15(1):S1–S12, 2007. pdf, DOI.
- [38] V. P. Smyshlyaev and N. A. Fleck . The role of strain gradients in the grain size effect for polycrystals. *Journal of Mechanics and Physics of Solids*, 44:465–495, 1996. pdf, doi.
- [39] Y. Wei and J.W. Hutchinson. Steady-state crack growth and work of fracture for solids characterized by strain gradient plasticity. *Journal of the Mechanics and Physics of Solids*, 45(21):1253–1273, August 1997. pdf, doi.



- [40] G.N. Wells, K. Garikipati, and L. Molari. A discontinuous Galerkin method for strain gradient-dependent damage. *Computer Methods in Applied Mechanics and Engineering*, 193:3633–3645, 2004. pdf, DOI.
- [41] Z.C. Xia and J. W. Hutchinson. Crack tip fields in strain gradient plasticity . *Journal of Mechanics and Physics of Solids*, 44:1621–1648, 1996. pdf, doi.



# Appendix A

## Strain Gradient Constitutive Relations

The strain gradient constitutive relations used here are taken from Wei Y. and Hutchinson J.W. [39], Fleck and Hutchinson [10] The strain gradient constitutive relation is expressed as

$$\tau_{ijk} = \frac{\partial W}{\partial \eta_{ijk}} \quad (\text{A.1})$$

the strain gradient constitutive relation in a linear form can be written as

$$W = \frac{1}{2} \lambda \epsilon_{ii} \epsilon_{jj} + \mu \epsilon_{ij} \epsilon_{ij} + \mu \left( c_1 \eta_{ijk}^{(1)} \eta_{ijk}^{(1)} + c_2 \eta_{ijk}^{(2)} \eta_{ijk}^{(2)} + c_3 \eta_{ijk}^{(3)} \eta_{ijk}^{(3)} + c_4 \eta_{ijk}^H \eta_{ijk}^H \right) \quad (\text{A.2})$$

From the strain energy density function the higher order stress can be written in terms on strain gradients as

$$\tau_{ijk} = J_{ijklmn} \eta_{lmn} \quad (\text{A.3})$$

Where  $J_{ijklmn}$  is given as

$$J_{ijklmn} = 2El_e^2 \sum_{I=1}^4 \kappa_e^{(I)^2} T_{ijklmn}^{(I)} \quad (\text{A.4})$$

where  $T_{ijklmn}^{(I)}$ 's are given by

$$\begin{aligned} T_{ijkpqr}^{(1)} &= \frac{1}{6} \{ (\delta_{ip}\delta_{jq} + \delta_{iq}\delta_{jp}) \delta_{kr} + (\delta_{jp}\delta_{kq} + \delta_{jq}\delta_{kp}) \delta_{ir} + (\delta_{ip}\delta_{kq} + \delta_{iq}\delta_{kp}) \delta_{jr} \} \\ &\quad - \frac{1}{15} \{ (\delta_{ij}\delta_{kr} + \delta_{jk}\delta_{ir} + \delta_{ki}\delta_{jr} + \delta_{ki}\delta_{jr}) \delta_{pq} \} \\ &\quad - \frac{1}{15} \{ (\delta_{ij}\delta_{kp} + \delta_{jk}\delta_{ip} + \delta_{ki}\delta_{jp}) \delta_{qr} + (\delta_{ij}\delta_{kq} + \delta_{jk}\delta_{iq} + \delta_{ki}\delta_{jq}) \delta_{rp} \} \end{aligned} \quad (\text{A.5})$$

$$\begin{aligned} T_{ijkpqr}^{(2)} &= \frac{1}{12} \{ e_{ikq}e_{jpr} + e_{jkq}e_{ipr} + e_{ikp}e_{jqr} + e_{jkp}e_{iqr} \} \\ &\quad + \frac{1}{12} \{ 2(\delta_{ip}\delta_{jq} + \delta_{iq}\delta_{jp}) \delta_{kr} - (\delta_{jp}\delta_{kq} + \delta_{jq}\delta_{kp}) \delta_{ir} - (\delta_{ip}\delta_{kq} + \delta_{iq}\delta_{kp}) \delta_{jr} \} \end{aligned} \quad (\text{A.6})$$

$$\begin{aligned} T_{ijkpqr}^{(3)} &= -\frac{1}{12} \{ e_{ikq}e_{jpr} + e_{jkq}e_{ipr} + e_{ikp}e_{jqr} + e_{jkp}e_{iqr} \} \\ &\quad - \frac{1}{8} \{ (\delta_{ip}\delta_{jk} + \delta_{jp}\delta_{ik}) \delta_{qr} + (\delta_{iq}\delta_{kj} + \delta_{jq}\delta_{ik}) \delta_{pr} \} \\ &\quad + \frac{1}{12} \{ 2(\delta_{ip}\delta_{jq} + \delta_{iq}\delta_{jp}) \delta_{kr} - (\delta_{jp}\delta_{kq} + \delta_{jq}\delta_{kp}) \delta_{ir} - (\delta_{ip}\delta_{kq} + \delta_{iq}\delta_{kp}) \delta_{jr} \} \end{aligned} \quad (\text{A.7})$$

$$T_{ijkpqr}^{(4)} = \frac{1}{8} \{ (\delta_{ik}\delta_{jp} + \delta_{jk}\delta_{ip}) \delta_{qr} + (\delta_{ik}\delta_{jq} + \delta_{jk}\delta_{iq}) \delta_{pr} \} \quad (\text{A.8})$$

# Appendix B

## Derivation of the upper bound of the bilinear form

The bilinear  $a(\mathbf{u}, \mathbf{w})$  form for the non-local linear elastic problem is

$$\begin{aligned} a(\mathbf{u}, \mathbf{w}) &= \int_{B_{0h}} w_{k,i} \sigma_{ik} d\Omega + \int_{B_{0h}} w_{k,ij} \tau_{jik} d\Omega \\ &+ \int_{\partial_I \Omega} \llbracket w_{k,i} \rrbracket \left( \langle \tau_{jik} \rangle n_j + n_j \left\langle \frac{\beta J_{jikqrp}}{h} \right\rangle \llbracket u_{p,q} \rrbracket n_r \right) dS \end{aligned} \quad (\text{B.1})$$

and  $b(\mathbf{w})$  given by

$$b(\mathbf{w}) = \int_{B_{0h}} w_k b_k d\Omega + \int_{\partial_N \Omega} w_k t_k dS + \int_{\partial_M \Omega} w_{k,l} n_l r_k dS \quad (\text{B.2})$$

Using triangular inequality on equation (B.1)

$$\begin{aligned}
|a(\mathbf{u}, \mathbf{w})| &\leq \left| \int_{B_{0h}} w_{k,i} \sigma_{ik} d\Omega \right| + \left| \int_{B_{0h}} w_{k,ij} \tau_{jik} d\Omega \right| + \left| \int_{\partial_I \Omega} \llbracket w_{k,i} \rrbracket \langle \tau_{jik} \rangle n_j dS \right| \\
&\quad + \left| \int_{\partial_I B_{0h}} \llbracket w_{k,i} \rrbracket n_j \left\langle \frac{\beta J_{jikqrp}}{h} \right\rangle \llbracket u_{p,q} \rrbracket n_r dS \right|
\end{aligned} \tag{B.3}$$

Applying Cauchy-Schwartz inequality to the first term of (B.3) we have

$$\begin{aligned}
\left| \int_{B_{0h}} w_{k,i} \sigma_{ik} d\Omega \right| &\leq \sum_e \left| \int_{\Omega_e} w_{k,i} \sigma_{ik} d\Omega \right| \\
&\leq \sum_e \left\| \sqrt{C_{ijkl}} w_{k,l} \right\|_{L^2(\Omega^e)} \left\| \sqrt{C_{ijkl}} u_{i,j} \right\|_{L^2(\Omega^e)}
\end{aligned} \tag{B.4}$$

Similarly, applying Cauchy-Schwartz inequality to the higher order stress term

$$\begin{aligned}
\left| \int_{B_{0h}} w_{k,ij} \tau_{jik} d\Omega \right| &\leq \sum_e \left| \int_{\Omega_e} w_{k,ij} \tau_{jik} d\Omega \right| \\
&\leq \sum_e \left\| \sqrt{J_{jikqrp}} w_{k,ij} \right\|_{L^2(\Omega^e)} \left\| \sqrt{J_{jikqrp}} u_{p,qr} \right\|_{L^2(\Omega^e)}
\end{aligned} \tag{B.5}$$

The quadratic term can be bounded by

$$\begin{aligned}
&\left| \int_{\partial_I B_{0h}} \llbracket w_{k,i} \rrbracket n_j \left\langle \frac{\beta J_{jikqrp}}{h} \right\rangle \llbracket u_{p,q} \rrbracket n_r dS \right| \\
&\leq \frac{\beta}{2} \sum_e \left\| \sqrt{\frac{J_{jikqrp}}{h}} w_{k,i} n_j^- \right\|_{L^2(\partial\Omega^e \cap \partial_I B_h)} \left\| \sqrt{\frac{J_{jikqrp}}{h}} u_{p,q} n_r^- \right\|_{L^2(\partial\Omega^e \cap \partial_I B_h)}
\end{aligned} \tag{B.6}$$

and, finally the consistency term.

$$\begin{aligned}
& \left| \int_{\partial_I \Omega} \llbracket w_{k,i} \rrbracket \langle \tau_{jik} \rangle n_j dS \right| = \frac{1}{2} \sum_e \left| \int_{\partial \Omega_e \cap \partial_I \Omega} \llbracket w_{k,i} \rrbracket \langle \tau_{jik} \rangle n_j dS \right| \\
& \leq \frac{1}{2} \sum_e \left\| h_s^{\frac{1}{2}} \sqrt{J_{jikqrp}} \langle u_{p,qr} \rangle \right\|_{L^2(\partial \Omega_e \cap \partial_I B_h)} \left\| h_s^{-\frac{1}{2}} \llbracket w_{k,i} \rrbracket \sqrt{J_{jikqrp}} n_j^- \right\|_{L^2(\partial \Omega_e \cap \partial_I B_h)} \\
& \leq \sum_e \left\| h_s^{\frac{1}{2}} \sqrt{J_{jikqrp}} \langle u_{p,qr} \rangle \right\|_{L^2(\partial \Omega_e \cap \partial_I B_h)} \left\| h_s^{-\frac{1}{2}} \llbracket w_{k,i} \rrbracket \sqrt{J_{jikqrp}} n_j^- \right\|_{L^2(\partial \Omega_e \cap \partial_I B_h)} \\
& \leq C^k \sum_e \left\| \sqrt{J_{jikqrp}} u_{p,qr} \right\|_{L^2(\Omega^e)} \left\| h_s^{-\frac{1}{2}} \llbracket w_{k,i} \rrbracket \sqrt{J_{jikqrp}} n_j^- \right\|_{L^2(\partial \Omega_e \cap \partial_I B_h)}
\end{aligned} \tag{B.7}$$

Substituting (B.4)-(B.7) into (B.3) we obtain

$$\begin{aligned}
|a(\mathbf{u}, \mathbf{w})| & \leq \sum_e \left\| \sqrt{C_{ijkl}} w_{k,l} \right\|_{L^2(\Omega^e)} \left\| \sqrt{C_{ijkl}} u_{i,j} \right\|_{L^2(\Omega^e)} \\
& + \sum_e \left\| \sqrt{J_{jikqrp}} w_{k,ij} \right\|_{L^2(\Omega^e)} \left\| \sqrt{J_{jikqrp}} u_{p,qr} \right\|_{L^2(\Omega^e)} \\
& + \frac{\beta}{2} \sum_e \left\| \sqrt{\frac{J_{jikqrp}}{h}} w_{k,i} n_j^- \right\|_{L^2(\partial \Omega_e \cap \partial_I B_h)} \left\| \sqrt{\frac{J_{jikqrp}}{h}} u_{p,q} n_r^- \right\|_{L^2(\partial \Omega_e \cap \partial_I B_h)} \\
& + C^k \sum_e \left\| \sqrt{J_{jikqrp}} u_{p,qr} \right\|_{L^2(\Omega^e)} \left\| h_s^{-\frac{1}{2}} \llbracket w_{k,i} \rrbracket \sqrt{J_{jikqrp}} n_j^- \right\|_{L^2(\partial \Omega_e \cap \partial_I B_h)} \\
& \leq C_1(\beta) \sum_e \left\| \sqrt{C_{ijkl}} w_{k,l} \right\|_{L^2(\Omega^e)} \left\| \sqrt{C_{ijkl}} u_{i,j} \right\|_{L^2(\Omega^e)} \\
& + C_1(\beta) \sum_e \left\| \sqrt{J_{jikqrp}} w_{k,ij} \right\|_{L^2(\Omega^e)} \left\| \sqrt{J_{jikqrp}} u_{p,qr} \right\|_{L^2(\Omega^e)} \\
& + C_1(\beta) \sum_e \left\| \sqrt{\frac{J_{jikqrp}}{2h}} w_{k,i} n_j^- \right\|_{L^2(\partial \Omega_e \cap \partial_I B_h)} \left\| \sqrt{\frac{J_{jikqrp}}{2h}} u_{p,q} n_r^- \right\|_{L^2(\partial \Omega_e \cap \partial_I B_h)} \\
& + C_1(\beta) \sum_e \left\| \sqrt{J_{jikqrp}} u_{p,qr} \right\|_{L^2(\Omega^e)} \left\| h_s^{-\frac{1}{2}} \llbracket w_{k,i} \rrbracket \sqrt{J_{jikqrp}} n_j^- \right\|_{L^2(\partial \Omega_e \cap \partial_I B_h)}
\end{aligned} \tag{B.8}$$

with  $C_1^k(\beta) = \max(1, \beta, \sqrt{2}C^k)$ . This essentially gives us

$$\begin{aligned}
\frac{|a(\mathbf{u}, \mathbf{w})|}{C_1(\beta)} &\leq \sum_e \left\| \sqrt{C_{ijkl}} w_{k,l} \right\|_{L^2(\Omega^e)} \left\| \sqrt{C_{ijkl}} u_{i,j} \right\|_{L^2(\Omega^e)} \\
&+ \sum_e \left\| \sqrt{J_{ijkqrp}} w_{k,ij} \right\|_{L^2(\Omega^e)} \left\| \sqrt{J_{ijkqrp}} u_{p,qr} \right\|_{L^2(\Omega^e)} \\
&+ \sum_e \left\| \sqrt{\frac{J_{jikqrp}}{2h}} w_{k,i} n_j^- \right\|_{L^2(\partial\Omega^e \cap \partial_I B_h)} \left\| \sqrt{\frac{J_{jikqrp}}{2h}} u_{p,q} n_r^- \right\|_{L^2(\partial\Omega^e \cap \partial_I B_h)} \\
&+ \sum_e \left\| \sqrt{J_{ijkqrp}} u_{p,qr} \right\|_{L^2(\Omega^e)} \left\| h_s^{-\frac{1}{2}} \llbracket w_{k,i} \rrbracket \sqrt{J_{jikqrp}} n_j^- \right\|_{L^2(\partial\Omega^e \cap \partial_I B_h)}
\end{aligned} \tag{B.9}$$

The idea here is to get an expression for the upper bound of the bilinear  $a(\mathbf{u}, \mathbf{w})$  in terms of the energy norm of  $\mathbf{u}$  and  $\mathbf{w}$  so we collect terms depending on  $\mathbf{u}$  and  $\mathbf{w}$  and we obtain,

$$\begin{aligned}
\frac{|a(\mathbf{u}, \mathbf{w})|}{C_1(\beta)} &\leq \sum_e \left[ \left\| \sqrt{C_{ijkl}} u_{i,j} \right\|_{L^2(\Omega^e)} + \left\| \sqrt{J_{ijkqrp}} u_{p,qr} \right\|_{L^2(\Omega^e)} \right. \\
&\quad \left. + \left\| \sqrt{\frac{J_{jikqrp}}{2h}} \llbracket u_{p,q} \rrbracket n_r^- \right\|_{L^2(\partial\Omega^e \cap \partial_I B_h)} \right] \times \\
&\quad \left[ \left\| \sqrt{C_{ijkl}} w_{i,j} \right\|_{L^2(\Omega^e)} + \left\| \sqrt{J_{ijkqrp}} w_{p,qr} \right\|_{L^2(\Omega^e)} \right. \\
&\quad \left. + \left\| \sqrt{\frac{J_{jikqrp}}{2h}} \llbracket w_{p,q} \rrbracket n_r^- \right\|_{L^2(\partial\Omega^e \cap \partial_I B_h)} \right]
\end{aligned} \tag{B.10}$$



Squaring both sides of the equation (B.10) and applying Cauchy-Schwartz inequality to (B.10) we get-

$$\begin{aligned}
\frac{|a(\mathbf{u}, \mathbf{w})|^2}{C_1^2(\beta)} &\leq \sum_e \left[ \left\| \sqrt{C_{ijkl}} u_{i,j} \right\|_{L^2(\Omega^e)} + \left\| \sqrt{J_{jikqrp}} u_{p,qr} \right\|_{L^2(\Omega^e)} \right. \\
&\quad \left. + \left\| \sqrt{\frac{J_{jikqrp}}{2h}} \llbracket u_{p,q} \rrbracket n_r^- \right\|_{L^2(\partial\Omega^e \cap \partial_I B_h)} \right]^2 \times \\
&\quad \left[ \left\| \sqrt{C_{ijkl}} w_{i,j} \right\|_{L^2(\Omega^e)} + \left\| \sqrt{J_{jikqrp}} w_{p,qr} \right\|_{L^2(\Omega^e)} \right. \\
&\quad \left. + \left\| \sqrt{\frac{J_{jikqrp}}{2h}} \llbracket w_{p,q} \rrbracket n_r^- \right\|_{L^2(\partial\Omega^e \cap \partial_I B_h)} \right]^2
\end{aligned} \tag{B.11}$$

noting that  $a^2 + b^2 \geq 2ab$  we obtain.

$$\begin{aligned}
\frac{|a(\mathbf{u}, \mathbf{w})|^2}{9C_1^2(\beta)} &\leq \sum_e \left[ \left\| \sqrt{C_{ijkl}} u_{i,j} \right\|_{L^2(\Omega^e)}^2 + \left\| \sqrt{J_{jikqrp}} u_{p,qr} \right\|_{L^2(\Omega^e)}^2 \right. \\
&\quad \left. + \left\| \sqrt{\frac{J_{jikqrp}}{2h}} \llbracket u_{p,q} \rrbracket n_r^- \right\|_{L^2(\partial\Omega^e \cap \partial_I B_h)}^2 \right] \times \\
&\quad \left[ \left\| \sqrt{C_{ijkl}} w_{i,j} \right\|_{L^2(\Omega^e)}^2 + \left\| \sqrt{J_{jikqrp}} w_{p,qr} \right\|_{L^2(\Omega^e)}^2 \right. \\
&\quad \left. + \left\| \sqrt{\frac{J_{jikqrp}}{2h}} \llbracket w_{p,q} \rrbracket n_r^- \right\|_{L^2(\partial\Omega^e \cap \partial_I B_h)}^2 \right]
\end{aligned} \tag{B.12}$$

Equation (B.12) can be expressed using 3.51 as,

$$|a(\mathbf{u}, \mathbf{w})|^2 \leq C^k(\beta) \|\mathbf{u}\|^2 \|\mathbf{w}\|^2 \tag{B.13}$$



# Appendix C

## Convergence Analysis- discontinuous Galerkin method

Using the definition of energy norm (3.51), the energy norm for error in the interpolated spaces can be written as

$$\begin{aligned} \|\mathbf{u} - \mathbf{u}^k\| = & \left\| \sqrt{\mathbf{C}} : \nabla (\mathbf{u} - \mathbf{u}^k) \right\|_{L^2(\Omega_0)}^2 + \left\| \sqrt{\mathbf{J}} : \nabla^2 (\mathbf{u} - \mathbf{u}^k) \right\|_{L^2(\Omega_0)}^2 \\ & + \sum_e \frac{1}{2} \left\| \sqrt{\frac{\mathbf{J}}{h}} : \nabla ([[\mathbf{u} - \mathbf{u}^k]]) \otimes \mathbf{n}^- \right\|_{L^2(\partial\Omega^e \cap \partial_I B_h)}^2 \end{aligned} \quad (\text{C.1})$$

We have dropped the tensor indices for the sake of brevity .The first term of (C.1) can be bounded by

$$\begin{aligned}
\left\| \sqrt{\mathbf{C}} : \nabla (\mathbf{u} - \mathbf{u}^k) \right\|_{L^2(\Omega_0)}^2 &\leq \left\| \sqrt{\mathbf{C}} \right\|_{L^2(\Omega_0)}^2 \left\| \nabla (\mathbf{u} - \mathbf{u}^k) \right\|_{L^2(\Omega_0)}^2 \\
&\leq C_1 \left\| \nabla (\mathbf{u} - \mathbf{u}^k) \right\|_{L^2(\Omega_0)}^2 \\
&\leq C_1 \left\| (\mathbf{u} - \mathbf{u}^k) \right\|_{H^1(\Omega_0)}^2 \\
&\leq C_2 h_s^{2k} |\mathbf{u}|_{H^{k+1}(\Omega_0)}^2
\end{aligned} \tag{C.2}$$

Here we have assumed positive definiteness of  $C$ , applied the property  $\|\mathbf{a} \cdot \mathbf{b}\| \leq \|\mathbf{a}\| \|\mathbf{b}\|$ , the definition of the Sobolev space  $\|u_{,x}\|_{H^0(\Omega_0)} \leq \|u\|_{H^1(\Omega_0)}$  and the basic error estimates of interpolation theory. Similarly the second term of the right hand side of (C.1) can be shown to become

$$\left\| \sqrt{\mathbf{J}} : \nabla^2 (\mathbf{u} - \mathbf{u}^k) \right\|_{L^2(\Omega_0)}^2 \leq C_2 h_s^{2k-2} |\mathbf{u}|_{H^{k+1}(\Omega_0)}^2 \tag{C.3}$$

Additionally we employ the inverse inequality the inverse inequality<sup>1</sup> and the positive

---

<sup>1</sup>  $\forall m \geq l \exists C_I > 0 : \|v\|_{\mathbf{H}^m(\Omega_0)} \leq C_I h_s^{l-m} \|v\|_{\mathbf{H}^l(\Omega_0)}$ .

definiteness of  $\mathbf{J}$  to obtain (C.3). Now the third term of (C.1), one has:

$$\begin{aligned}
& \sum_e \frac{1}{2} \left\| \sqrt{\frac{\mathbf{J}}{h_e}} : \nabla (\llbracket \mathbf{u} - \mathbf{u}^k \rrbracket) \otimes \mathbf{n}^- \right\|_{L^2(\partial\Omega^e \cap \partial_I B_h)}^2 = \\
& \sum_e \left\| \sqrt{\frac{\mathbf{J}}{h_e}} : \nabla (\mathbf{u} - \mathbf{u}^k) \otimes \mathbf{n}^- \right\|_{L^2(\partial_I B_h)}^2 \leq \\
& C_3 h_e^{-1} \sum_e \|\nabla (\mathbf{u} - \mathbf{u}^k) \otimes \mathbf{n}^-\|_{L^2(\partial_I B_h)}^2 \leq \\
& \sum_e \frac{C_4}{h_e^2} \|(\mathbf{u} - \mathbf{u}^k)_{,\alpha}\|_{L^2(\partial\Omega^e)}^2 + \sum_e C_5 \|(\mathbf{u} - \mathbf{u}^k)_{,\alpha\beta}\|_{L^2(\partial\Omega^e)}^2 \leq \\
& \sum_e \frac{C_4}{h_e^2} \|(\mathbf{u} - \mathbf{u}^k)\|_{\mathbf{H}^1(\partial\Omega^e)}^2 + \sum_e C_5 \|(\mathbf{u} - \mathbf{u}^k)\|_{\mathbf{H}^2(\partial\Omega^e)}^2 \leq \\
& \sum_e \frac{C_6}{h_e^4} \|(\mathbf{u} - \mathbf{u}^k)\|_{L^{2^2}(\partial\Omega^e)}^2 \leq \sum_e C h_e^{2k-2} |\mathbf{u}|_{\mathbf{H}^{k+1}(\partial\Omega^e)}^2
\end{aligned} \tag{C.4}$$

Combining the last three results the energy norm of the error can be written as

$$\|e\|^2 = \sum_e C h_e^{2k-2} |\mathbf{u}|_{\mathbf{H}^{k+1}(\partial\Omega^e)}^2 \tag{C.5}$$



# Appendix D

## Implementation of second order derivatives of the element shape functions

The Finite element interpolated displacement inside each element is given as,

$$u_i = \sum_a^n N_a U_{ai} \quad (\text{D.1})$$

where  $N$  is the shape function and  $U$  are the nodal displacements. Differentiating with respect to the spatial coordinate system

$$\frac{\partial u_i}{\partial x_j} = \sum_{a=1}^n \sum_{k=1}^3 \frac{\partial N_a}{\partial \xi_k} \frac{\partial \xi_k}{\partial x_j} U_{ai} \quad (\text{D.2})$$

where  $\xi_k$  are the isoparametric mapped space. From this the derivative of shape function can be written as

$$\frac{\partial N_a}{\partial x_j} = \sum_{k=1}^3 \frac{\partial N_a}{\partial \xi_k} \frac{\partial \xi_k}{\partial x_j} \quad (\text{D.3})$$

Taking the second derivative,

$$\begin{aligned} \frac{\partial^2 u_i}{\partial x_j \partial x_k} &= \frac{\partial}{\partial x_k} \left( \sum_{a=1}^n \sum_{l=1}^3 \frac{\partial N_a}{\partial \xi_l} \frac{\partial \xi_l}{\partial x_j} U_{ai} \right) \\ &= \left( \sum_{a=1}^n \sum_{l=1}^3 \left( \frac{\partial}{\partial x_k} \left( \frac{\partial N_a}{\partial \xi_l} \right) \frac{\partial \xi_l}{\partial x_j} + \frac{\partial N_a}{\partial \xi_l} \frac{\partial^2 \xi_l}{\partial x_j \partial x_k} \right) \right) U_{ai} \\ &= \left( \sum_{a=1}^n \sum_{l=1}^3 \left( \sum_{m=1}^3 \left( \frac{\partial^2 N_a}{\partial \xi_l \partial \xi_m} \right) \frac{\partial \xi_l}{\partial x_j} \frac{\partial \xi_m}{\partial x_k} + \frac{\partial N_a}{\partial \xi_l} \frac{\partial^2 \xi_l}{\partial x_j \partial x_k} \right) \right) U_{ai} \quad (\text{D.4}) \end{aligned}$$

The second derivative of shape function can thus be written as

$$\frac{\partial^2 N_a}{\partial x_j \partial x_k} = \sum_{l=1}^3 \left( \sum_{m=1}^3 \left( \frac{\partial^2 N_a}{\partial \xi_l \partial \xi_m} \right) \frac{\partial \xi_l}{\partial x_j} \frac{\partial \xi_m}{\partial x_k} + \frac{\partial N_a}{\partial \xi_l} \frac{\partial^2 \xi_l}{\partial x_j \partial x_k} \right) \quad (\text{D.5})$$

For a 10 node tetrahedral element  $\frac{\partial N}{\partial \xi}$  will have 30 terms and  $\frac{\partial^2 N}{\partial \xi^2}$  will have 90 terms.

Going to a cubic element will produce a horrible number of derivatives to compute.

To compute  $\frac{\partial^2 \xi}{\partial x^2}$ , we start with computing  $\frac{\partial \xi}{\partial x}$ , which can be obtained by solving the



following linear equations.

$$\underbrace{\begin{pmatrix} \sum_a x_a \frac{\partial N_a}{\partial \xi_1} & \sum_a x_a \frac{\partial N_a}{\partial \xi_2} & \sum_a x_a \frac{\partial N_a}{\partial \xi_3} \\ \sum_a y_a \frac{\partial N_a}{\partial \xi_1} & \sum_a y_a \frac{\partial N_a}{\partial \xi_2} & \sum_a y_a \frac{\partial N_a}{\partial \xi_3} \\ \sum_a z_a \frac{\partial N_a}{\partial \xi_1} & \sum_a z_a \frac{\partial N_a}{\partial \xi_2} & \sum_a z_a \frac{\partial N_a}{\partial \xi_3} \end{pmatrix}}_A \begin{pmatrix} \frac{\partial \xi_1}{\partial x} & \frac{\partial \xi_1}{\partial y} & \frac{\partial \xi_1}{\partial z} \\ \frac{\partial \xi_2}{\partial x} & \frac{\partial \xi_2}{\partial y} & \frac{\partial \xi_2}{\partial z} \\ \frac{\partial \xi_3}{\partial x} & \frac{\partial \xi_3}{\partial y} & \frac{\partial \xi_3}{\partial z} \end{pmatrix} = \begin{pmatrix} 1 & 0 & 0 \\ 0 & 1 & 0 \\ 0 & 0 & 1 \end{pmatrix} \quad (\text{D.6})$$

$$\begin{pmatrix} \frac{\partial \xi_1}{\partial x} & \frac{\partial \xi_1}{\partial y} & \frac{\partial \xi_1}{\partial z} \\ \frac{\partial \xi_2}{\partial x} & \frac{\partial \xi_2}{\partial y} & \frac{\partial \xi_2}{\partial z} \\ \frac{\partial \xi_3}{\partial x} & \frac{\partial \xi_3}{\partial y} & \frac{\partial \xi_3}{\partial z} \end{pmatrix} = \begin{pmatrix} \sum_a x_a \frac{\partial N_a}{\partial \xi_1} & \sum_a x_a \frac{\partial N_a}{\partial \xi_2} & \sum_a x_a \frac{\partial N_a}{\partial \xi_3} \\ \sum_a y_a \frac{\partial N_a}{\partial \xi_1} & \sum_a y_a \frac{\partial N_a}{\partial \xi_2} & \sum_a y_a \frac{\partial N_a}{\partial \xi_3} \\ \sum_a z_a \frac{\partial N_a}{\partial \xi_1} & \sum_a z_a \frac{\partial N_a}{\partial \xi_2} & \sum_a z_a \frac{\partial N_a}{\partial \xi_3} \end{pmatrix}^{-1} \quad (\text{D.7})$$

$\frac{\partial \xi_i}{\partial x_j}$  can thus be written as,

$$\frac{\partial \xi_i}{\partial x_j} = \hat{A}_{ij} \quad (\text{D.8})$$

where  $\hat{A}_{ij} = (A^{-1})_{ij}$ , is the inverse of  $A$ . Now, starting with the first derivative of the coordinate transformation, the second derivative can be computed as-

$$\begin{aligned} \frac{\partial}{\partial x_k} \left( \frac{\partial \xi_i}{\partial x_j} \right) &= \frac{\partial}{\partial x_k} \left( \hat{A}_{ij} \right) \\ &= \sum_{m=1}^3 \frac{\partial}{\partial \xi_m} \left( \hat{A}_{ij} \right) \frac{\partial \xi_m}{\partial x_k} \\ &= - \sum_{m=1}^3 \sum_{o=1}^3 \sum_{n=1}^3 \hat{A}_{in} \frac{\partial A_{no}}{\partial \xi_m} \hat{A}_{oj} \hat{A}_{mk} \end{aligned} \quad (\text{D.9})$$

$\frac{\partial A_{no}}{\partial \xi_m}$  can be computed starting from  $A_{no}$ ,

$$A_{no} = \sum_{a=1}^n x_{na} \frac{\partial N_a}{\partial \xi_o} \quad (\text{D.10})$$

differentiating with respect to  $\xi_j$  the expression obtained is,

$$\frac{\partial A_{no}}{\partial \xi_j} = \sum_{a=1}^n x_{na} \frac{\partial^2 N_a}{\partial \xi_o \partial \xi_j} \quad (\text{D.11})$$

If the mid-nodes of the tetrahedral are inserted at the mid points of the corner nodes then the term  $\frac{\partial A_{no}}{\partial \xi_j}$  in (D.11) would go to zero thus making the second derivative of the jacobian of the coordinate mapping  $\frac{\partial}{\partial x_k} \left( \frac{\partial \xi_i}{\partial x_j} \right)$  equal to zero.

# Appendix E

## Analytical solutions for 1-D strain gradient problems

### E.1 Uni-axial tensile load

The analytical solution is derived for a uniform linear elastic strain gradient prismatic beam of length  $L$  subjected to tensile load. The beam is clamped at one end  $x = 0$  and subjected to a displacement load at the other end. The Young's modulus is  $E$  and the length scale parameter is  $l$ , the governing differential equation for static equilibrium of the beam is

$$E (u_{,xx} - l^2 u_{,xxxx}) = 0 \quad (\text{E.1})$$

The general solution to the above ODE is given as

$$u(x) = A_1 x + A_2 + B_1 \sinh\left(\frac{x}{l}\right) + B_2 \cosh\left(\frac{x}{l}\right) \quad (\text{E.2})$$

An unique solution can be obtained by applying the boundary conditions, since the governing equilibrium equation is fourth order, four boundary conditions have to be enforced and which are

$$u(0) = 0 \tag{E.3}$$

$$u(L) = \delta \tag{E.4}$$

$$u''(L) = 0 \tag{E.5}$$

$$u''(0) = 0 \tag{E.6}$$

$$\tag{E.7}$$

It is worth noting that the boundary conditions (E.5) and (E.6) correspond to the double stress traction being zero. Substituting the boundary conditions in equation (E.3) and (E.6) into the balance equation (E.1), the displacement field for the problem can be obtained as

$$u(x) = \frac{x}{L}\delta, x \in [0, L] \tag{E.8}$$

## E.2 Bi-material subjected to uni-axial tensile load

An analytical solution is presented for a bimaterial, consisting of two dissimilar linear elastic strain gradient solids. The bimaterial is subjected to tensile loading applied in the form of a displacement boundary condition. The Youngs moduli of the two material being  $E^+$  and  $E^-$  respectively. The internal length scale  $l$  and the nonlocal constants  $c1, c2, c3, c4$  are taken to be the same on both sides. We reduce the governing

differential equations into one dimension and the resulting equation is given as

$$E(u_{,xx} - l^2 u_{,xxxx}) = 0 \quad (\text{E.9})$$

The general solution to the above ordinary differential equation is

$$u^+(\xi) = A_1^+ \xi + A_2^+ + B_1^+ \sinh\left(\frac{\xi}{l}\right) + B_2^+ \cosh\left(\frac{\xi}{l}\right) \quad \forall \xi \leq 0 \quad (\text{E.10})$$

$$u^-(\xi) = A_1^- \xi + A_2^- + B_1^- \sinh\left(\frac{\xi}{l}\right) + B_2^- \cosh\left(\frac{\xi}{l}\right) \quad \forall \xi \geq 0 \quad (\text{E.11})$$

An unique solution can be obtained by using the interface and boundary conditions.

The interface conditions being, continuity of displacements, continuity of first derivate of displacement, continuity of tractions and continuity of higher order tractions.

$$[u(0)] = 0 \quad (\text{E.12})$$

$$[u_{,x}(0)] = 0 \quad (\text{E.13})$$

$$[Eu_{,x}(0) - El^2 u_{,xxx}(0)] = 0 \quad (\text{E.14})$$

$$[El^2 u_{,xx}(0)] = 0 \quad (\text{E.15})$$

The boundary conditions being

$$u\left(-\frac{L}{2}\right) = 0 \quad (\text{E.16})$$

$$u\left(\frac{L}{2}\right) = U \quad (\text{E.17})$$

$$(\text{E.18})$$

$$u_{xx}\left(-\frac{L}{2}\right) = 0 \quad (\text{E.19})$$

$$u_{xx}\left(\frac{L}{2}\right) = 0 \quad (\text{E.20})$$

The particular solution satisfying all these conditions are

$$A_1^+ = \frac{\mu U}{\alpha}, A_2^+ = U\left(1 - \frac{\mu L}{2\alpha}\right), B_1^+ = -\frac{\mu\beta U}{\alpha}, B_2^+ = \mu \tanh\left(\frac{L}{2l}\right) \frac{\beta}{\alpha} U \quad (\text{E.21})$$

$$A_1^- = \frac{U}{\alpha}, A_2^- = \frac{LU}{2\alpha}, B_1^- = \frac{\beta}{\alpha} U, B_2^- = \tanh\left(\frac{L}{2l}\right) \frac{\beta}{\alpha} U \quad (\text{E.22})$$

where  $\alpha = \frac{L}{2}(1 + \mu) - l \tanh\left(\frac{L}{2l}\right) \frac{(1-\mu)^2}{(1+\mu)}$ ,  $\beta = \frac{l(\mu-1)}{(1+\mu)}$  and  $\mu = \frac{E^-}{E^+}$

The strain profile across the length of the domain is plotted for various values of  $\frac{l}{L}$ , figure (E.1). For very small values of  $\frac{l}{L}$ , the strain profile is close to the linear elasticity solution and for large values of  $\frac{l}{L}$  the bi-material sample behaves like a homogeneous medium under static loading conditions.

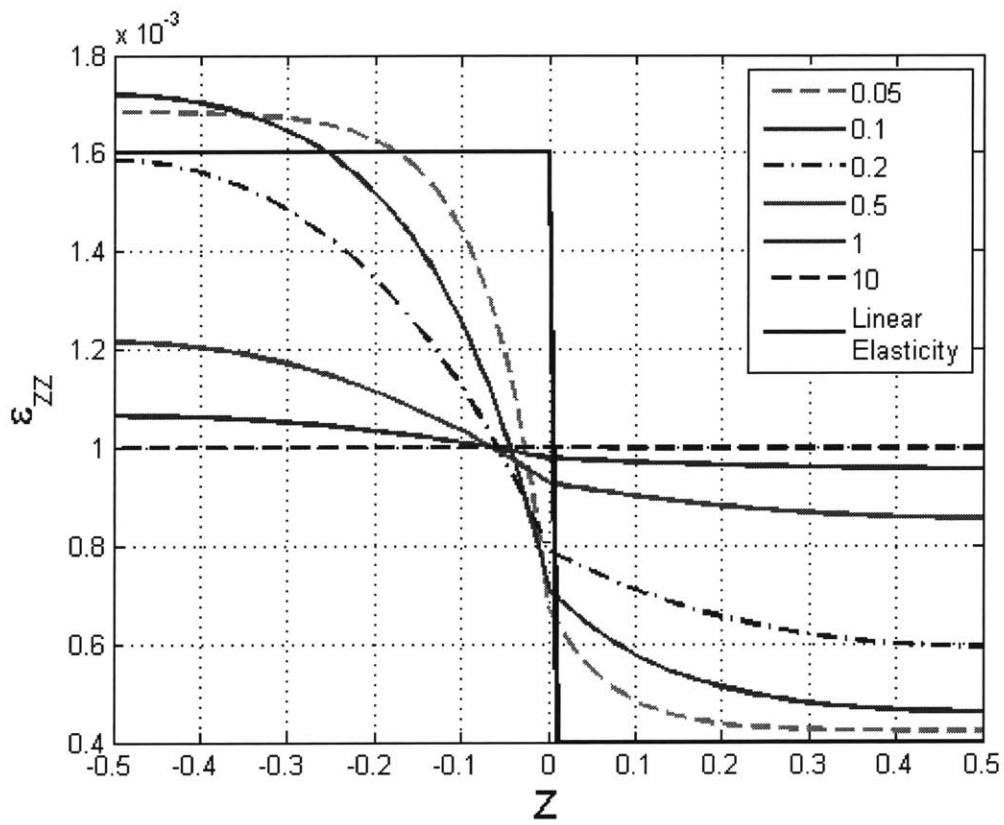


Figure E.1: Comparison of strain profile in the domain for the the variation of  $\frac{l}{L}$